Identification of SPP1-positive macrophages by single-cell spatial analysis in human lung tissues with mycobacterial infection

Harutaka Katano[1*], Akira Hebisawa[2], Yuko Sato[1], Yoshihiko Hoshino[3*]

[1]Department of Pathology, National Institute of Infectious Diseases, Tokyo 162-8640, Japan.
[2]Clinical Research Center, National Hospital Organization Tokyo National Hospital, Tokyo 204-8585, Japan.
[3]Department of Mycobacteriology, Leprosy Research Center, National Institute of Infectious Diseases, Tokyo 189-0002, Japan.

*Corresponding authors. Email: katano@niid.go.jp and yhoshino@niid.go.jp

Brief summary

SPP1-CD44 signaling in SPP1-positive macrophages may play a role in granuloma formation in mycobacterial and other granulomatous diseases.

Short title: SPP1+ macrophage in mycobacterial infection

Abstract

Tuberculosis and non-tuberculous mycobacterial (NTM) diseases are infections caused by *Mycobacterium tuberculosis* and non-tuberculous mycobacteria such as the *Mycobacterium avium* complex, leading to the formation of granulomatous lesions with caseous necrosis in the lungs. Although granulomatous tissues are infiltrated by numerous inflammatory cells, including macrophages, lymphocytes, and neutrophils, the mechanisms underlying granuloma formation caused by mycobacteria remain unclear. In this study, we performed single-cell spatial analysis on lung tissue samples from patients with tuberculosis and NTM diseases to investigate the infiltrating cell populations. We analyzed seven lung lesions and identified individual cell types infiltrating the granulomatous tissue. Based on gene expression profiles, at least four macrophage subtypes were identified. Notably, SPP1-positive macrophages predominantly found infiltrating the granulomatous tissue. Langhans giant cells expressed SPP1, and numerous SPP1-positive macrophages without giant cell morphology were also observed around the granulomas. RNA-seq analysis revealed elevated SPP1 expression in mycobacterium-infected tissues. The SPP1-CD44 signaling pathway was active in SPP1-positive macrophages and their neighboring cells in mycobacterium-infected tissues. SPP1-positive macrophages were also observed around granulomas in other granulomatous diseases, such as granulomatosis with polyangiitis and sarcoidosis. These findings suggest that SPP1-CD44 signaling in SPP1-positive macrophages may play a role in the pathology of granulomatous diseases, including mycobacterial infections.

INTRODUCTION

Tuberculosis and non-tuberculous mycobacterial (NTM) diseases, caused by *Mycobacterium tuberculosis* and various non-tuberculous mycobacteria—particularly the *Mycobacterium avium intracellulare* complex (MAC)—represent significant public health challenges(*1*). These infections predominantly affect the lungs, leading to the formation of granulomatous lesions, which are characterized by caseous necrosis(*2*). Despite extensive research efforts, the mechanisms underlying granuloma formation in mycobacterial infections remain largely enigmatic and poorly understood(*3-5*).

Granulomas are highly organized structures that form in response to persistent pathogens. These cellular conglomerates, composed of immune cells such as macrophages, lymphocytes, and neutrophils, aim to contain and neutralize the pathogen, serving as a barrier to prevent its spread(*2, 4, 6*). Immunohistochemical and special staining techniques have detected mycobacterial antigens within the caseous necrotic tissue of granulomas, supporting the hypothesis that granulomas play a crucial role in controlling the dissemination of mycobacteria(*3*). However, the precise formation and dynamic regulation of these structures, particularly in the context of mycobacterial infections, remain incompletely understood.

Various immune cells, including macrophages, B cells, T cells, NK cells, dendritic cells, and neutrophils, participate in granuloma formation.(*2, 7*). Among these, macrophages are pivotal, exhibiting remarkable plasticity that allows them to adapt to a wide range of environmental stimuli. During mycobacterial infections, macrophages can assume diverse functional states, contributing both to pathogen clearance and, paradoxically, to pathogen survival(*3, 4, 8, 9*). Macrophages, along with dendritic cells and alveolar epithelial cells, phagocytize mycobacteria during the initial stages of infection. The immune response to mycobacteria triggers several signaling pathways, including IFN-γ and TLR2 signaling, which promote the production of pro-inflammatory cytokines such as IL-12, IL-23, and TNF-α. These signals, particularly through TLR2, ultimately contribute to the formation of granulomas.(*8, 10-13*).

To gain insight into the cellular responses to mycobacterial infections in the lung, it is critical to identify the specific cell types infiltrating granulomas and to characterize their dynamic interactions. To this end, we employed the cutting-edge Nanostring CosMx™ platform to perform single-cell spatial analysis on lung tissue samples from patients with MTB or NTM diseases. This advanced technology enabled us to map and identify individual cell types

surrounding the granulomatous tissue(*14*). In addition, single-cell spatial analysis allowed for detailed gene expression profiling within individual cells, providing insights into the localization of cells and the identification of key signaling pathways involved in cell-cell communication within the tissue microenvironment. This innovative approach holds promise for unraveling the complex interplay of immune cells during MTB and NTM infections.

In our study, we applied single-cell spatial analysis to explore the cellular landscape of lung tissue samples from patients with MTB or NTM infections, with a particular emphasis on macrophages and their critical role in granuloma formation.

RESULTS

Cell typing in lung tissues with mycobacterial infection

Seven lung tissue samples from patients with MTB (n = 3) and NTM (n = 4) infections were analyzed using the Nanostring CosMx™ platform (Fig. 1A and table S1). Each slide contained granulomas with inflammatory cell infiltrates, including foreign body macrophages (Langhans giant cells, figs. S1a and S1b). Immunohistochemistry and Ziehl-Neelsen staining demonstrated that mycobacteria bacilli were predominantly localized at the center of granulomas and absent from the surrounding inflammatory cell infiltrates in both NTM and MTB samples (fig. S2). The CosMx™ platform enables multiplex gene quantification for 960 genes in formalin-fixed paraffin-embedded (FFPE) slides with a documented sensitivity of 1-2 gene copies per cell and spatial transcript localization precision of less than 50 nm, corresponding to single cell resolution (*14*). CosMx™ analysis identified a total of 300,841 cells across the seven slides (table S3). After cell segmentation, transcription signals by in situ hybridization were detected in each cell on the slide (average: 131 transcripts per cell, Fig. 1B and table S3). All cells were clustered based on transcript expression profiles. Differentially expressed gene (DEG) analysis identified 520 cluster-specific marker genes with adjusted p-values. A total of 26 distinct clusters were identified (Fig. 1C and fig. S3A), which were visualized using uniform manifold approximation and projection (UMAP, Fig. 1D and fig. S3B). These DEGs (gene lists available in Supplementary Data: marker_heatmap_nb_clus_4.csv) were used to annotate subpopulations. The cell types within each cluster were determined by SingleR. Neutrophil and B-cell lineages were manually annotated based on gene expression data from the Human Gene Atlas (Gene Set Enrichment Analysis, GSEA, https://www.gsea-msigdb.org/gsea/index.jsp). All

cells in each focus of view (fov) from the seven slides were annotated and labeled by colors in spatial images (Fig. 1E).

Through in silico analysis based on gene expression, 3 types of T cells were identified as CD4+, CD8+ cytotoxic, and regulatory T cells (fig. S4A). Three B-cell clusters were identified as B cells, plasma cells and B-cell linage cells. The cluster of B-cell lineage cluster exhibited gene expression patterns similar to plasma cells with J-chain expression being higher in plasma cells than B-cell lineage cluster (fig. S4B). Fibroblasts were categorized into three subtypes (a-c) based on varying collagen expression levels, including COL1A1 and COL3A1 (fig. S4C). Four macrophage subtypes (a-d) were identified, categorized based on the expression of specific markers such as CD14, CD163, CD68, and LYZ. Subtypes *a*, *b*, and *c* corresponding to M1 macrophages, M2 macrophage with low CD14 expression, and M2 macrophage with high CD14 expression, respectively (Figs. 2A and 2B). Macrophage subtype *d*, which expressed CCR7 and lacked CD163 expression (indicating an M1 phenotype), predominantly expressed SPP1 and MARCO (Figs. 2A-D). In violin, dot plots, and UMAP (Fig. 2), SPP1 expression appeared more specific to macrophage subtype d than MARCO and FN1, leading to its designation as SPP1-positive macrophages. The proportions of cell types varied across samples and FoVs (Fig. S5, Table S4). B cells (including B cells, B-cell lineage cells, and plasma cells) and fibroblasts (subtypes a–c) were the most abundant cell types, comprising 12.25% and 21.94% of the total cell population, respectively. Macrophages (subtypes a–d) and T cells (CD4+, CD8+, and Treg) accounted for 14.88% and 9.55% of the total cells, respectively. SPP1-positive macrophages (subtype d) represented 3.18% of all cells across the slides.

SPP1-positive macrophages infiltrate around MTB and NTM granulomas

CosMx™ spatial imaging revealed the cell types around granulomas. While numerous CD4 and CD8 T cells, B cells and macrophages infiltrated to interstitial regions and area around granulomas, macrophages were predominantly detected in the regions adjacent to granulomas (Fig. 3). Notably, SPP1-positive macrophages predominantly infiltrated the periphery of NTM-positive granulomatous tissue (Fig. 3 and figs. S6a and S6b). In MTB-infected tissues, SPP1-positive macrophages were also observed in the interstitial regions and alveolar spaces (Fig. 4 and fig. S6c). Immunohistochemistry using an anti-SPP1 antibody demonstrated that SPP1 expression was localized in the cytoplasm of Langhans giant cells (Figs. 3C and 4C), suggesting that these giant cells represent a form of SPP1-positive macrophages. Furthermore, CosMx™ spatial imaging and immunohistochemistry indicated

that SPP1 was present in macrophages lacking giant cell morphology, located around mycobacterium-positive granulomas in close proximity to Langhans giant cells (Figs. 3A–3C). This observation suggests that SPP1-positive macrophages without giant cell morphology may share a similar origin with Langhans giant cells.

Bulk RNA-seq analysis of RNA extracted from mycobacterium-infected tissues also revealed elevated expression of SPP1 in infected tissues compared to controls (figs. S7A-7C). Gene ontology analysis indicated that cytokine-mediated signaling pathways and extracellular matrix organization were upregulated in mycobacterium-infected samples (fig. S7D). These processes involved high expression of SPP1 and CD44, respectively.

Ligand-receptor interaction of SPP1

Using spatial transcriptome data, the R package InSituCor swas employed for spatial correlation analysis to detect significant ligand-receptor interactions in the samples (fig. S8). This analysis identified SPP1, FN1, and MARCO as co-expression markers of SPP1-positive macrophages (Fig. 5A). Furthermore, InSituCor detected SPP1-CD44 and FN1-CD44 pairs as active ligand-receptor interactions in both NTM and MTB samples (Fig. 5B). Correlation network analysis using InSituCor identified numerous molecules involved in the SPP1-CD44 network (Fig. 5C). Spatial imaging of these samples demonstrated that CD44-positive cells were localized near SPP1-positive macrophages; however CD44-positive cells were distributed more broadly compared to SPP1-positive macrophages (fig. S9). Spatial analysis further revealed co-expression of CD44 and SPP1 in SPP1-positive macrophages (macrophage_d) within tissues infected with mycobacteria (Figs. 5D and 5E). Co-expression of SPP1 and CD44, as well as SPP1-CD44 ligand-receptor signaling, was frequently detected around granulomatous regions (fig. S10).

Dot plot analysis showed that CD44 was expressed by a variety of cell types, including macrophages, mast cells, CD8+ T cells, and dendritic cells around the granulomatous lesions, while SPP1 expression was predominantly confined to the macrophage_d subtype (Fig. 6A). Immunohistochemistry for SPP1 and CD44 showed SPP1 and CD44 expression in Langhans giant cells and various cells around SPP1-positive macrophages, respectively (Fig. 6B). Spatial imaging using the CosMx™ platform confirmed that CD44 was expressed not only in macrophages but also in various cell types, including B cells, T cells, and epithelial cells surrounding SPP1-positive macrophages (Fig. 6C). Immunofluorescence assay further confirmed that CD44 expression in SPP1-positive large foreign body macrophages and their surrounding cells (Fig. 6C). The SPP1-CD44 interaction was additionally identified using the

CellChat package (Fig. 7). SPP1, expressed by macrophage_d, was shown to interact with various cell types. Circle plots and heatmaps of the SPP1 signaling pathway network indicated that the receiver cells for the SPP1-CD44 signal included macrophage_d, macrophage_c, and occasionally CD8+ cytotoxic T cells, while the sender cell was macrophage_d (SPP1-positive macrophage) (Figs. 7B, 7C, 7E, and 7G). The receiver cells of the SPP1-CD44 signaling pathway varied among samples (Fig. 7C). Although macrophages were the primary receiver cells, B cells, CD8+ T cells, and alveolar epithelial cells also acted as receivers in certain cases. Beyond the SPP1-CD44 signaling pathway, other significant cell communication pathways identified by CellChat included collagen, MHC-I, MIF, FN1, integrin β2, PECAM1, and ICAM pathways (Fig. 7D, fig. S11). The incoming and outgoing interactions of the SPP1-CD44 pathway by macrophage_d were relatively strong among the cell types and other pathways in mycobacterium-infected tissues (Figs. 7A, 7F, and 7G, fig. S11). In the SPP1-CD44 signaling pathway, SPP1 expressed by macrophage_d communicated with macrophage_d itself, mast cells, and CD8+ T cells (Figs. 7E-7G and fig. S11).

SPP1-positive macrophages in granuloma associated with non-mycobacterial infection

To determine whether SPP1-positive macrophages are associated with granulomatous diseases beyond mycobacterial infections, pathological samples from granulomatous lesions in patients with rheumatoid nodule (RN), granulomatosis with polyangiitis (GPA), sarcoidosis (SA), Aspergillus pneumonia (AP), and aspiration pneumonia (Aspi-P) were examined. Immunohistochemistry revealed that SPP1 was present in some foreign body giant macrophages surrounding the granulomatous lesions across all tested samples (Fig. 8). RNA-seq analysis of RNA extracted from these granulomatous samples demonstrated elevated expression of SPP1 in the granulomatous lesions, similar to the expression levels observed in mycobacterial infections, compared with control lung and tonsil samples (fig. S7C). Expression of CD40L (CD154) and CD40 pair, another ligand-receptor pair reported as activation in granulomatous diseases(*15*), did not show significant difference between granulomatous samples and controls (Fig. 5B). Furthermore, immunohistochemistry revealed CD44 expression in SPP1-positive macrophages and neighboring cells within the lesions of GPA, SA, RN, and AP (Figs. 8A and 8B). Immunofluorescence imaging also demonstrated that a subset of SPP1-positive macrophages expressed CD44 (Fig. 8C). These findings suggest that SPP1-positive macrophages are broadly associated with granulomatous diseases, and that the SPP1-CD44 interaction is observed commonly in granulomatous

pathology.

DISCUSSION

A pivotal discovery in our study was the identification of multiple macrophage subtypes within the tissues of granulomatous diseases. Based on gene expression patterns, we identified at least four distinct macrophage cell types. Among these, SPP1-positive macrophages predominantly infiltrated the regions surrounding NTM- and MTB-positive granulomatous tissue. Additionally, we found that Langhans giant cells were a specialized form of these SPP1-positive macrophages. Notably, besides these giant cells, we observed a significant number of SPP1-positive macrophages that did not exhibit giant cell morphology, indicating a diverse range of morphologies for these cells.

Our spatial transcriptomics data demonstrated that at least 26 types of cells infiltrated the lungs with mycobacterial infection (Fig.1). Although the percentages of infiltrating cell types varied among samples, macrophages were predominant cell types adjacent to granuloma regions in all seven samples. Along with macrophages, T cells, B cells, plasma cells, and dendritic cells were also observed around granuloma. These cell populations are consistent with those reported in MTB and NTM tissues in previous studies (*2-9*). Macrophages have been shown to be key player in granuloma formation (*5, 7, 10*). Various macrophage subtypes infiltrate granulomas alongside T and B cells in mycobacterial infections, with M1/M2 macrophage polarization inducing NF-kappa B activation, which is associated with granuloma formation and outcome(*10*).

SPP1, also known as osteopontin, is a multifunctional secreted phosphorylated glycoprotein produced by macrophages and T cells. It is associated with bone remodeling, T cell and B cell activation, and chemotaxis(*16-20*). SPP1 expression in foreign body macrophages, such as Langhans giant cells, has been previously reported in pathological samples from tuberculosis and sarcoidosis (*16, 21-24*). However, there are no reports describing macrophages without large cell morphology expressing SPP1 around granulomas. Given that SPP1-positive macrophages share a similar transcript profile with Langhans giant cells and are categorized within the same cluster (Fig. 3), some of these cells may subsequently fuse to form Langhans giant cells. Recent studies using single cell transcriptomics and/or spatial omics assay have highlighted the potential role of SPP1-positive macrophages in infections, inflammatory diseases and cancer (*25, 26*). For instance, in tissue samples from a patient with

granulomatous slack skin, CD11c+/LYZ+ macrophages exhibited an M1-like phenotype and strongly expressed MMP9, MMP12, CHI3L1, CHIT1, COL1A1, TIMP1, and SPP1, all of which are involved in extracellular matrix degradation and tissue remodeling (*27*). SPP1-positive macrophages have also been detected in bronchoalveolar lavage fluid from tuberculosis patients (*28*). Interestingly, plasma osteopontin levels are higher in patients with tuberculosis and sarcoidosis compared to healthy donors (*29, 30*). A study on perivascular adipose tissue in heart transplant recipients demonstrated the presence of SPP1-positive macrophages in the perivascular tissues, with an identified interaction between secreted SPP1 and CD44 (*31*). These data suggest that SPP1-positive macrophages secrete SPP1 and induce SPP1-CD44 signaling in inflammation. In a *Schistosoma mansoni* egg-induced granuloma animal model, granulomas from osteopontin-knockout animals were smaller and contained significantly fewer macrophages, as well as fewer macrophage-derived epithelioid cells and giant cells (*32*). Thus, the presence of SPP1-positive macrophages in granulomatous tissues suggests an important role for SPP1 in granuloma formation through its interactions.

In our study, we demonstrated that the SPP1-CD44 pathway was one of the main ligand-receptor pairs involved in cell-cell communication in granulomatous lesions (Fig. 7). Recent studies have shown that SPP1 is associated with cancer cell growth and resistance to chemoradiotherapy, inducing epithelial-mesenchymal transition, autophagy, aberrant glucose metabolism, epigenetic alterations, and reduced drug uptake through the SPP1-CD44 signaling (*33*). SPP1-positive macrophages have been identified in colorectal cancer and squamous cell carcinoma(*34, 35*). In hepatocellular cancer, SPP1-positive macrophages infiltrated hypoxic tumor regions with cancer stem cells, where the SPP1 signaling pathway was highly active in cell-cell communication with SPP1-CD44 and SPP1-ITGA/ITGB identified as the main ligand-receptor pairs (*36*). SPP1 also binds to integrins α4β1, α9β1, and α9β4, inducing cell adhesion and migration. CD44 has also been identified as a receptor for SPP1, and the SPP1-CD44 signaling pathway has been reported in various cancers(*37-39*). SPP1-positive macrophages have been detected in cancers as tumor-associated macrophages, and the SPP1-CD44 pathway has been identified as a critical mediator of communication between tumor-associated macrophage subpopulations (*40-42*). The SPP1-CD44 pathway has been linked to cancer chemoresistance in solid tumors and to cell-to-cell communication between cancer cells and tumor-associated macrophages (*36, 43, 44*). The presence of SPP1-positive macrophages in cancers correlates with worse prognosis and poor immunotherapy response, leading to reduced survival (*36, 40*). Some therapeutic approaches

targeting SPP1-CD44 signaling have been reported in vitro and in vivo. In a mouse model, SPP1 was shown to induce cancer cell chemoresistance by activating the CD44 receptor, and that treatment with anti-SPP1 and anti-CD44 antibodies improved cancer cell sensitivity to cisplatin (*45*). Importantly, the SPP1-CD44 signaling pathway has been identified as a potential immune checkpoint target(*46, 47*). CD44 expression in tumor cells was positively correlated with PD-L1 expression and the numbers of infiltrated CD68- and CD168-positive macrophages(*48*). It was also demonstrated that SPP1-CD44 immune checkpoint regulates CD8+ T cell activation and tumor immune evasion in interferon regulatory factor 8 deficient mice (*46*). Inhibition of the SPP1-CD44 pathway, therefore, may be a potential therapeutic strategy to reduce granuloma formation in granulomatous diseases, such as mycobacterial infections. In tuberculosis and MAC infections, granulomas encapsulate mycobacteria in necrotic tissue to prevent their spread. Since granuloma formation is a major characteristic of mycobacterial infections, further studies will be required to explore the inhibition of the SPP1-CD44 pathway in macrophages.

In conclusion, our study sheds light on the intricate cellular dynamics involved in granuloma formation in mycobacterial diseases. The prominence of SPP1-positive macrophages, including Langhans giant cells, suggests that SPP1-CD44 pathway in these cells may play a role in this process, opening avenues for further research and potential therapeutic interventions.

MATERIALS AND METHODS

Tissue samples

FFPE samples of resected lung tissues from patients with active mycobacterial diseases, granulomatous diseases, or other controls were used (table S1). For CosMx™ spatial molecular imaging (SMI) analysis(*14*), 7 lung resections were obtained from 3 MTB and 4 NTM patients undergoing lung resection surgery. Total 28 lung tissues from 25 patients were applied to histological analysis, immunohistochemistry and RNAseq analysis by next generation sequencing. In addition, five intact lung tissues from patients with cancer and four tonsillar tissues were used as controls. All MTB and NTM were diagnosed as active disease by sputum culture and/or PCR method. The study was approved by the Ethics Committee of National Institute of Infectious Diseases (approval no. 1781) and National Hospital Organization Tokyo National Hospital (approval no. 408).

Single cell spatial transcriptomics

Spatial transcriptomic profiling of FFPE lung sections was performed using the CosMx™ Spatial Molecular Imager, as previously described (*14*). The CosMx™ Human Universal Cell Characterization RNA Panel (1000-plex; Nanostring, Seattle, WA) was applied to seven FFPE samples, including three tuberculosis samples, three MAC-positive pneumonia samples, and one MAC-negative bronchiectasis sample with 15-45 fields of view (fov) per sample, totaling 216 fovs (Table S3). Fovs measuring 0.512 mm × 0.512 mm were used for the commercial instrument in the final runs (MTB2, MTB3, NTM3), whereas fovs measuring 0.985 mm × 0.657 mm were used for the development instrument in the remaining samples (MTB1, NTM1, NTM2, NTM4). Fovs were placed on the tissue to align with regions of interest identified by H&E staining of an adjacent serial section. Fovs were selected from areas around granuloma or inflammatory cell infiltration to avoid granulomatous necrotic tissues. The mean area explored was 4.60 mm^2 per sample. Sample preparation and CosMx™ SMI instrument run was performed as described previously (*14, 25*). In addition to RNA readout, tissue samples were incubated with a fluorophore-conjugated antibody cocktail against CD298/B2M (488 nm), PanCK (532 nm), CD45 (594 nm), and either CD3 or CD68 (647 nm) proteins and DAPI stain. Cell segmentation, assigning transcripts at the cell-level, and obtaining a transcript by cell count matrix were performed as previously described (*14, 25*). Following total count normalization across all detected cells, highly variable genes (HVGs) were identified. Then, principal component analysis (PCA) was computed on the HVGs. Finally, uniform manifold approximation and projection (UMAP) was performed on these data(*14, 25*).

Cell type annotation

To identify subpopulation markers, we ran findMarkers (scran package, version 1.22.1)(*49*), blocking by sample, considering HVGs only, and testing for positive log-fold changes. The 100 top ranked genes were selected and passed to SingleR (version 1.8.1)(*50*).

Co-expression and cellular communication assay

Spatial correlation analysis such as co-expression and receptor-ligand assay was performed in the CosMx™ dataset with a R package InSituCor (*51*). InSituCor was run on normalized count data, adjusted for the effects of cell type, tissue ID and single cell counts, to uncover spatial correlations beyond those accounted for by these variables. Cellular communication

for cell types were also analyzed with CellChat (http://www.cellchat.org/). In CellChat, to convert spatial transcriptomics data of CosMx™, conversion.factor = 0.18 was used for setting spatial factors. In function "computeCommunProb", contact.range = 50 and scale.distance = 20 were used.

Bulk RNA-seq analysis of lung tissues

Total RNA was extracted from FFPE samples (Supplementary Table 1, 5 MTB, 7 NTM, 12 granulomatous diseases including 2 RN, 3 AP, 3 GPA, 3 SA, and 1 Aspi-P, 4 control lung, and 4 tonsils) with Quick-DNA/RNA FFPE Miniprep Kit (Zymo Research). Barcoded RNA-seq library was established with NEBNext Ultra II RNA Library Prep Kit for Illumina (New England BioLabs, Ipswich, MA) according to the manufacturer's instructions. Libraries were subjected to pair-end sequencing (300 cycles) on a Nextseq 1000 platform (Illumina, San Diego, CA). Quality filtering, adapter trimming, and RNAseq analyzing was performed using CLC genomics workbench (version 23, Qiagen, Hilden, Germany). Homo sapience refseq GRCh38.p13 was used as a reference genome of RNA sequences. PCA, volcano blot, and box plots were performed using the R (version 4.3.1) statistics package with RStudio (version 2023.06.1+524). Gene ontology assay was performed in biojupies (https://maayanlab.cloud/biojupies/analyze/).

Immunohistochemistry (IHC), immunofluorescence (IF), and special staining

Immunostaining was performed in the tissue sections of mycobacterial infection and other granulomatous diseases. Anti-SPP1 rabbit polyclonal antibody (HPA027541, Sigma-Aldrich, St. Louis, MO) and anti-CD44 mouse monoclonal antibody (UMAB134, OriGene Technologies, Rockville, MD) were used as primary antibodies. Anti-Bacillus Calmette–Guérin rabbit polyclonal antibody (B124, Dako, Copenhagen, Denmark) was used for detecting mycobacterial infection. For the second and third phase immunostaining reagents, a biotinylated F(ab')2 fragment of rabbit anti-mouse immunoglobulin (Dako) and peroxidase-conjugated streptavidin (Dako) were used. 3-3'diaminobenzidine was used as a chromogen and the slides were counterstained with hematoxylin. Nuclear counterstaining was performed with DAPI on IF samples. Image acquisition was performed on virtual slide system (VS200, Evident, Tokyo, Japan). The Ziehl-Neelsen stain was also performed to confirm mycobacterial infection.

Supplementary Materials

The PDF file includes:

Figs. S1 to S11

Tables S1 to S4

Other Supplementary Material for this manuscript includes the following:

marker_heatmap_nb_clus_4.csv

References

1. J. Furin, H. Cox, M. Pai, Tuberculosis. *Lancet* **393**, 1642-1656 (2019).
2. R. L. Hunter, Pathology of post primary tuberculosis of the lung: an illustrated critical review. *Tuberculosis (Edinb)* **91**, 497-509 (2011).
3. T. Ulrichs, S. H. Kaufmann, New insights into the function of granulomas in human tuberculosis. *J Pathol* **208**, 261-269 (2006).
4. S. Ehlers, U. E. Schaible, The granuloma in tuberculosis: dynamics of a host-pathogen collusion. *Front Immunol* **3**, 411 (2012).
5. D. G. Russell, P. J. Cardona, M. J. Kim, S. Allain, F. Altare, Foamy macrophages and the progression of the human tuberculosis granuloma. *Nat Immunol* **10**, 943-948 (2009).
6. B. Carow *et al.*, Immune mapping of human tuberculosis and sarcoidosis lung granulomas. *Front Immunol* **14**, 1332733 (2023).
7. M. J. Marakalala *et al.*, Inflammatory signaling in human tuberculosis granulomas is spatially organized. *Nat Med* **22**, 531-538 (2016).
8. H. E. Park *et al.*, Modulating macrophage function to reinforce host innate resistance against Mycobacterium avium complex infection. *Front Immunol* **13**, 931876 (2022).
9. P. L. Lin *et al.*, Sterilization of granulomas is common in active and latent tuberculosis despite within-host variability in bacterial killing. *Nat Med* **20**, 75-79 (2014).
10. S. Marino *et al.*, Macrophage polarization drives granuloma outcome during Mycobacterium tuberculosis infection. *Infect Immun* **83**, 324-338 (2015).
11. D. Smith, H. Hansch, G. Bancroft, S. Ehlers, T-cell-independent granuloma formation in response to Mycobacterium avium: role of tumour necrosis factor-alpha and interferon-gamma. *Immunology* **92**, 413-421 (1997).
12. P. J. Murray, Macrophage Polarization. *Annu Rev Physiol* **79**, 541-566 (2017).

13. M. Yoshida *et al.*, Transcriptome analysis of long non-coding RNAs in Mycobacterium avium complex-infected macrophages. *Front Immunol* **15**, 1374437 (2024).
14. S. He *et al.*, High-plex imaging of RNA and proteins at subcellular resolution in fixed tissue by spatial molecular imaging. *Nat Biotechnol* **40**, 1794-1806 (2022).
15. J. Villeneuve *et al.*, A Role for CD154, the CD40 Ligand, in Granulomatous Inflammation. *Mediators Inflamm* **2017**, 2982879 (2017).
16. A. W. O'Regan *et al.*, Osteopontin is associated with T cells in sarcoid granulomas and has T cell adhesive and cytokine-like properties in vitro. *J Immunol* **162**, 1024-1031 (1999).
17. S. T. Choi *et al.*, Osteopontin might be involved in bone remodelling rather than in inflammation in ankylosing spondylitis. *Rheumatology (Oxford)* **47**, 1775-1779 (2008).
18. F. P. Reinholt, K. Hultenby, A. Oldberg, D. Heinegard, Osteopontin--a possible anchor of osteoclasts to bone. *Proc Natl Acad Sci U S A* **87**, 4473-4475 (1990).
19. K. X. Wang, D. T. Denhardt, Osteopontin: role in immune regulation and stress responses. *Cytokine Growth Factor Rev* **19**, 333-345 (2008).
20. A. Koh *et al.*, Role of osteopontin in neutrophil function. *Immunology* **122**, 466-475 (2007).
21. I. Carlson, K. Tognazzi, E. J. Manseau, H. F. Dvorak, L. F. Brown, Osteopontin is strongly expressed by histiocytes in granulomas of diverse etiology. *Lab Invest* **77**, 103-108 (1997).
22. A. T. Tsai *et al.*, The role of osteopontin in foreign body giant cell formation. *Biomaterials* **26**, 5835-5843 (2005).
23. G. J. Nau *et al.*, A chemoattractant cytokine associated with granulomas in tuberculosis and silicosis. *Proc Natl Acad Sci U S A* **94**, 6414-6419 (1997).
24. D. Wang *et al.*, The association between osteopontin and tuberculosis: A systematic review and meta-analysis. *PLoS One* **15**, e0242702 (2020).
25. A. Garrido-Trigo *et al.*, Macrophage and neutrophil heterogeneity at single-cell spatial resolution in human inflammatory bowel disease. *Nat Commun* **14**, 4506 (2023).
26. L. MacDonald *et al.*, COVID-19 and RA share an SPP1 myeloid pathway that drives PD-L1+ neutrophils and CD14+ monocytes. *JCI Insight* **6**, (2021).

27. Y. Feng *et al.*, Spatial transcriptomics reveals heterogeneity of macrophages in the tumor microenvironment of granulomatous slack skin. *J Pathol* **261**, 105-119 (2023).
28. Q. Yang *et al.*, The interaction of macrophages and CD8 T cells in bronchoalveolar lavage fluid is associated with latent tuberculosis infection. *Emerg Microbes Infect* **12**, 2239940 (2023).
29. Y. Koguchi *et al.*, High plasma osteopontin level and its relationship with interleukin-12-mediated type 1 T helper cell response in tuberculosis. *Am J Respir Crit Care Med* **167**, 1355-1359 (2003).
30. J. Kadota *et al.*, High plasma concentrations of osteopontin in patients with interstitial pneumonia. *Respir Med* **99**, 111-117 (2005).
31. M. Fu *et al.*, Single-Cell RNA Sequencing of Coronary Perivascular Adipose Tissue From End-Stage Heart Failure Patients Identifies SPP1(+) Macrophage Subpopulation as a Target for Alleviating Fibrosis. *Arterioscler Thromb Vasc Biol* **43**, 2143-2164 (2023).
32. A. W. O'Regan *et al.*, Abnormal pulmonary granuloma formation in osteopontin-deficient mice. *Am J Respir Crit Care Med* **164**, 2243-2247 (2001).
33. C. Kretschmer *et al.*, Identification of early molecular markers for breast cancer. *Mol Cancer* **10**, 15 (2011).
34. R. Bill *et al.*, CXCL9:SPP1 macrophage polarity identifies a network of cellular programs that control human cancers. *Science* **381**, 515-524 (2023).
35. J. Qi *et al.*, Single-cell and spatial analysis reveal interaction of FAP(+) fibroblasts and SPP1(+) macrophages in colorectal cancer. *Nat Commun* **13**, 1742 (2022).
36. G. Fan *et al.*, Single-cell and spatial analyses revealed the co-location of cancer stem cells and SPP1+ macrophage in hypoxic region that determines the poor prognosis in hepatocellular carcinoma. *NPJ Precis Oncol* **8**, 75 (2024).
37. G. F. Weber, S. Ashkar, M. J. Glimcher, H. Cantor, Receptor-ligand interaction between CD44 and osteopontin (Eta-1). *Science* **271**, 509-512 (1996).
38. L. Liu *et al.*, Construction of TME and Identification of crosstalk between malignant cells and macrophages by SPP1 in hepatocellular carcinoma. *Cancer Immunol Immunother* **71**, 121-136 (2022).
39. C. Wang *et al.*, The heterogeneous immune landscape between lung adenocarcinoma and squamous carcinoma revealed by single-cell RNA sequencing. *Signal Transduct Target Ther* **7**, 289 (2022).

40. L. Xu *et al.*, Tumor-associated macrophage subtypes on cancer immunity along with prognostic analysis and SPP1-mediated interactions between tumor cells and macrophages. *PLoS Genet* **20**, e1011235 (2024).
41. H. He *et al.*, Multi-dimensional single-cell characterization revealed suppressive immune microenvironment in AFP-positive hepatocellular carcinoma. *Cell Discov* **9**, 60 (2023).
42. C. He *et al.*, Single-Cell Transcriptomic Analysis Revealed a Critical Role of SPP1/CD44-Mediated Crosstalk Between Macrophages and Cancer Cells in Glioma. *Front Cell Dev Biol* **9**, 779319 (2021).
43. W. Xie *et al.*, Multi-Transcriptomic Analysis Reveals the Heterogeneity and Tumor-Promoting Role of SPP1/CD44-Mediated Intratumoral Crosstalk in Gastric Cancer. *Cancers (Basel)* **15**, (2022).
44. P. Nallasamy *et al.*, Pancreatic Tumor Microenvironment Factor Promotes Cancer Stemness via SPP1-CD44 Axis. *Gastroenterology* **161**, 1998-2013 e1997 (2021).
45. J. Qian *et al.*, Cancer-associated mesothelial cells promote ovarian cancer chemoresistance through paracrine osteopontin signaling. *J Clin Invest* **131**, (2021).
46. J. D. Klement *et al.*, An osteopontin/CD44 immune checkpoint controls CD8+ T cell activation and tumor immune evasion. *J Clin Invest* **128**, 5549-5560 (2018).
47. C. Lu *et al.*, WDR5-H3K4me3 epigenetic axis regulates OPN expression to compensate PD-L1 function to promote pancreatic cancer immune escape. *J Immunother Cancer* **9**, (2021).
48. S. Liu *et al.*, CD44 is a potential immunotherapeutic target and affects macrophage infiltration leading to poor prognosis. *Sci Rep* **13**, 9657 (2023).
49. L. Haghverdi, A. T. L. Lun, M. D. Morgan, J. C. Marioni, Batch effects in single-cell RNA-sequencing data are corrected by matching mutual nearest neighbors. *Nat Biotechnol* **36**, 421-427 (2018).
50. D. Aran *et al.*, Reference-based analysis of lung single-cell sequencing reveals a transitional profibrotic macrophage. *Nat Immunol* **20**, 163-172 (2019).
51. P. Danaher *et al.*, Childhood-onset lupus nephritis is characterized by complex interactions between kidney stroma and infiltrating immune cells. *Sci Transl Med* **16**, eadl1666 (2024).

Acknowledgments

The authors thank Mike McKenna, Claire Williams, Patrick Danaher, Joseph M. Beechem, Nanostring USA, Fumiyo Kurokawa, Takayuki Taniya, and Takashi Uematsu, Nanostring Japan, and Ikuyo Yamamoto, Department of Pathology, National Institute of Infectious Diseases, for technical supports. The authors also thank Akiko Yamashita, Yukari Nogi, and Ginko Kaneda, Department of Mycobacteriology, National Institute of Infectious Diseases, for their assistance.

Funding

Japan Agency for Medical Research and Development (AMED) grant JP24fk0108701 (HK)
AMED grants JP23fk0108608, JP24fk0108673, JP24gm1610003, JP24gm1610007, JP24wm0125007, JP24wm0225022, JP24wm0325054, and JP24fk0108701 (YH)
Japan Society for the Promotion of Science (JSPS) for International Collaborative Research grant JP63KK0138 (YH)
JSPS Scientific Research grants JP24H00331, JP23K07665 and 23K07958 (YH)

Author contributions

Conceptualization: HK, YH
Methodology: HK, YS
Investigation: HK, AH, YS, YH
Visualization: HK, YH
Funding acquisition: HK, YH
Project administration: HK, YH
Supervision: HK, YH
Writing – original draft: HK, YH
Writing – review & editing: HK, AH, YS, YH

Competing interests

Authors declare that they have no competing interests.

Data and materials availability

Bulk RNA-seq and CosMx™ SMI raw data generated in this study have been deposited in

the GEO Omnibus database under accession code GSE276060 and GSE276083, respectively. The Seurat and Giotto objects of spatial analysis by CosMx™ SMI are registered in Figshare (https://figshare.com/). Full code for analysis of CosMx™ SMI data can be found at https://github.com/katanoh/Lung_CosMx_analysis.

Figure legends

Fig. 1. Single cell analysis of CosMx™ in mycobacterium-infected tissues. A. Overview of the study design for CosMx™ SMI, RNA-seq, and histological analysis. Lung samples, including MTB, NTM, granulomatous diseases and controls, were analyzed using RNA-seq (n = 37 samples) and CosMx™ SMI (n = 7 samples). This figure was created with BioRender.com. B. Representative image of CosMx™ SMI. All cells were segmented by segmentation markers and nuclei (upper panel). Transcripts (dots in various colors) were detected by in situ hybridization in each cell on the slides (lower panel). C. Dot plots showing expression of cell-typing markers in the indicated cell clusters. Dot size represents the percentage of cells expressing each gene in the cluster, while the average expression intensity of the markers is shown using a blue-to-red color gradient. D. UMAP plots of 300,841 cells from lung tissues with 4 NTM or 3 MTB patients. Each cluster is shown in a different color. E. Immunofluorescence image (upper panel) and spatial image obtained by CosMx™ SMI for MTB1 fov18 (lower panel). Cell annotations in the spatial image are listed in the right.

Fig. 2. Subtyping of macrophages. A. Violin plot showing macrophage-associated gene expression in macrophages and dendritic cells. B. Dot plot illustrating macrophage-associated gene expression specially in macrophages. C. UMAP plot depicting four macrophage subtypes. D. UMAP plot displaying the expression of macrophage-associated genes.

Fig. 3. Spatial images of SPP1-positive macrophages in MAC-positive lung tissues. (Case NTM2) A. HE staining (left panel), immunofluorescence (second panel), and CosMx™ spatial images (right two panels) of macrophage_d. Colors representing different cell types are shown in the right panel. In CosMx™ images, SPP1 and MARCO signals are indicated by green and red dots, respectively. Asterisk indicates granulomatous region. B. Enlarged images of the boxed regions in A. C. Immunohistochemistry for SPP1 in the same tissue near the granuloma. Asterisk indicates granulomatous region.

Fig. 4. CosMx™ spatial images of SPP1 and MARCO expression in macrophage_d in MTB tissue. (Case MTB1) A. Macrophage_d in the interstitial region expressed SPP1 and MARCO. B. Enlarged images of the boxed regions in A. C. Immunohistochemistry for SPP1 in the same tissue near the granuloma.

Fig. 5. Coexpression and ligand-receptor assay in InSituCor. A. Heatmap of co-expressed transcripts across different cell types. Co-expression of FN1, SPP1, and MARCO was specifically observed in macrophage_d (highlighted by the broken red line). B. Conditional correlation of ligand-receptor pairs in the ligand-receptor assay. The SPP1-CD44 and FN1-CD44 pairs show strong conditional correlations. C. Correlation network of SPP1 and CD44-associated transcripts. D. Spatial images showing SPP1-CD44 correlations in MTB and NTM tissues. Yellow indicates high correlation in the images (left: MTB1, right: NTM2). E. Spatial images from CosMx™ analysis of MTB and NTM samples. High expression of SPP1, CD44, and both are indicated by yellow, blue, and red dots, respectively.

Fig. 6. Expression of SPP1 and CD44 in macrophages around granuloma tissue with mycobacterial infection. A. Dot plot showing the expression of SPP1, MARCO, FN1, and CD44 across all cell types. B. Immunohistochemistry for SPP1 and CD44 in tissues from patients with MTB (upper panels) and NTM (lower panels) infections. C. Immunofluorescence and CosMx™ spatial images for SPP1 and CD44. SPP1 was expressed in the cytoplasm of multinuclear giant cells (immunofluorescence assay, left panels). CD44 expression was observed on the membrane of multinucleated giant cells and their neighboring cells. CosMx™ spatial images (right panels) showed that macrophage_d expresses both SPP1 and CD44. Colors representing different cell types are shown in the bottom right panel.

Fig. 7. Analysis of cellular communication among cell types using CellChat. A and B. Circular plots showing interactions among cell types in all pathways (A) and specifically in the SPP1 signaling pathway (B) across all seven cases analyzed with CosMx™. C. Circular plots depicting interactions among cell types in the SPP1 signaling pathway in each individual case. D. Histogram showing the relative contribution of each ligand-receptor (L-R) pair across all seven cases analyzed with CosMx™. Only significant L-R pairs are shown, with SPP1 interacting exclusively with CD44. E. Heatmap illustrating the signal intensity of the sender and receiver in the SPP1 signaling pathway across all samples. F. Dot plots showing the outgoing communication patterns of secreting cells. Significant outgoing signals in the identified signaling pathways are represented by dots. G. Dot plots showing the incoming communication patterns of secreting cells. Significant incoming signals are

represented by dots.

Fig. 8. SPP1 and CD44 expression in tissues from patients with granulomatous diseases. A. HE staining. B. Immunohistochemistry for SPP1. C. Immunofluorescence of SPP1 and CD44. Tissues from patients with sarcoidosis (left), granulomatosis with polyangiitis (GPA, middle), and rheumatoid nodule (RN, right) were investigated.

Fig.1

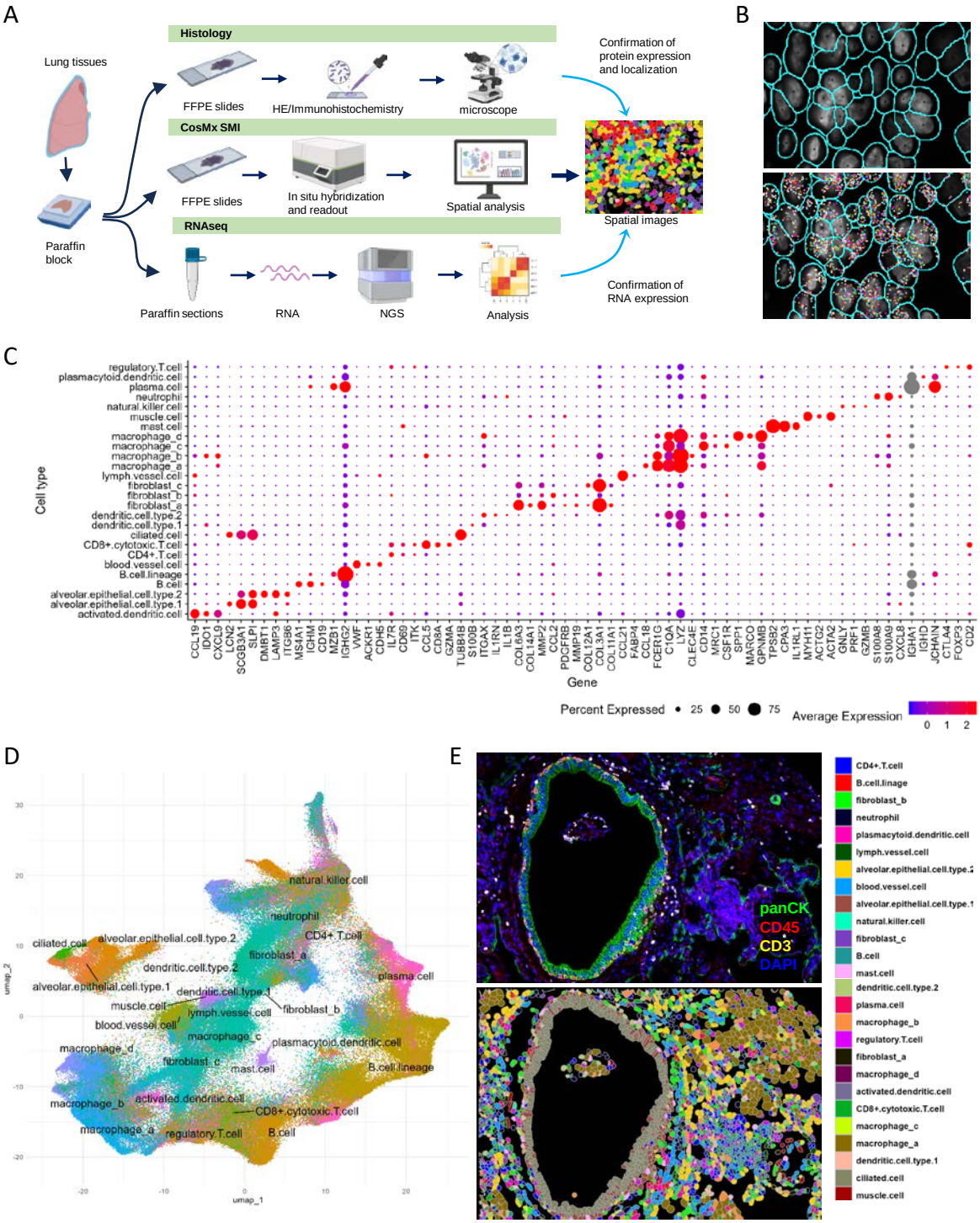
A
Lung tissues
Paraffin block
Histology
FFPE slides
HE/Immunohistochemistry
microscope
Confirmation of protein expression and localization
CosMx SMI
FFPE slides
In situ hybridization and readout
Spatial analysis
Spatial images
RNAseq
Paraffin sections
RNA
NGS
Analysis
Confirmation of RNA expression
B
C
Cell type
Gene
Percent Expressed
25
50
75
Average Expression
0
1
2
D
umap_1
umap_2
natural.killer.cell
neutrophil
CD4+.T.cell
ciliated.cell
alveolar.epithelial.cell.type.2
fibroblast_a
dendritic.cell.type.2
plasma.cell
alveolar.epithelial.cell.type.1
dendritic.cell.type.1
muscle.cell
lymph.vessel.cell
fibroblast_b
blood.vessel.cell
macrophage_c
plasmacytoid.dendritic.cell
macrophage_d
fibroblast_c
mast.cell
B.cell.lineage
macrophage_b
activated.dendritic.cell
CD8+.cytotoxic.T.cell
macrophage_a
regulatory.T.cell
B.cell
E
panCK
CD45
CD3
DAPI
CD4+.T.cell
B.cell.linage
fibroblast_b
neutrophil
plasmacytoid.dendritic.cell
lymph.vessel.cell
alveolar.epithelial.cell.type.2
blood.vessel.cell
alveolar.epithelial.cell.type.1
natural.killer.cell
fibroblast_c
B.cell
mast.cell
dendritic.cell.type.2
plasma.cell
macrophage_b
regulatory.T.cell
fibroblast_a
macrophage_d
activated.dendritic.cell
CD8+.cytotoxic.T.cell
macrophage_c
macrophage_a
dendritic.cell.type.1
ciliated.cell
muscle.cell

Fig.2

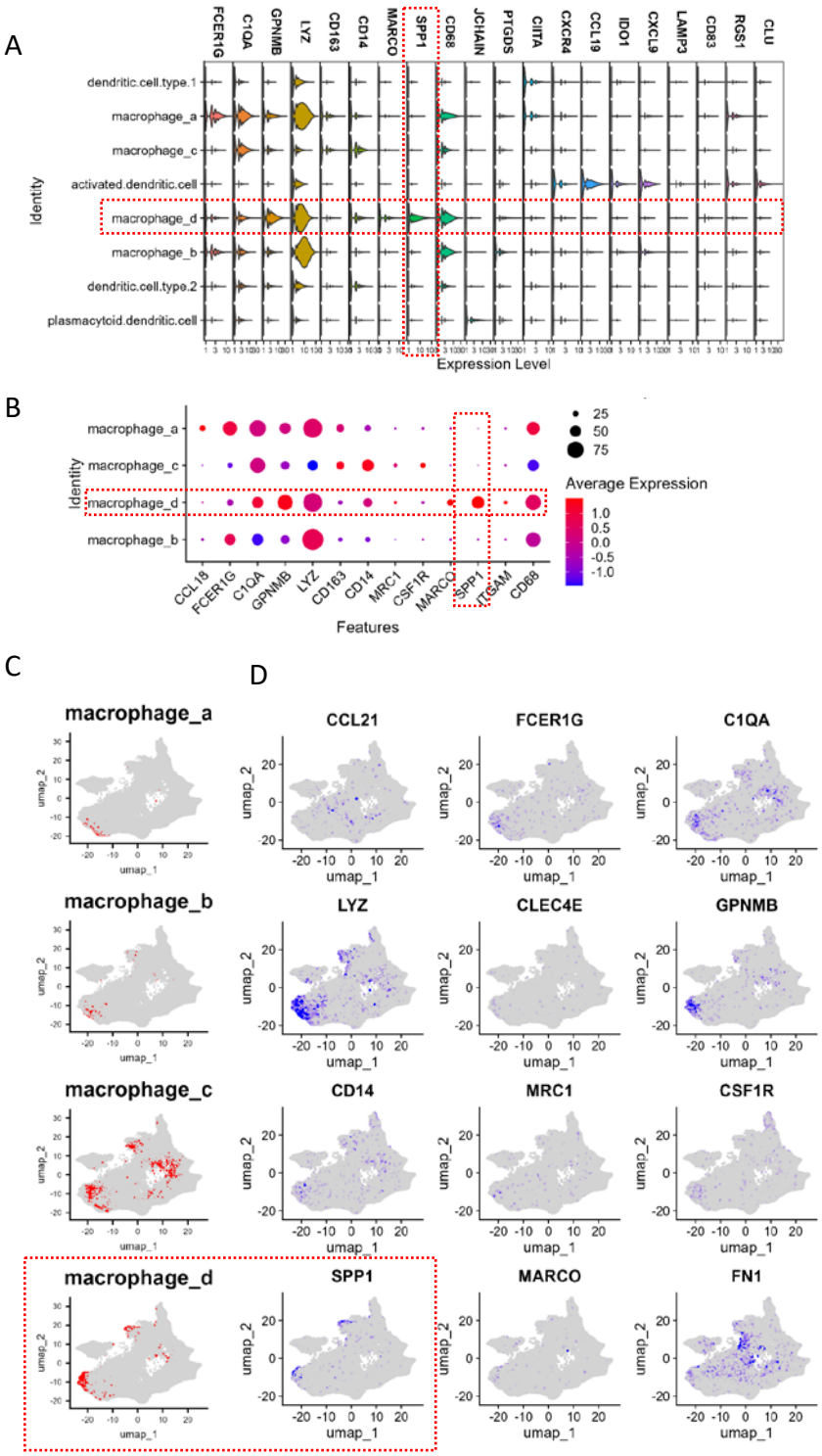
A
FCER1G
C1QA
GPNMB
LYZ
CD163
CD14
MARCO
SPP1
CD68
JCHAIN
PTGDS
CIITA
CXCR4
CCL19
IDO1
CXCL9
LAMP3
CD83
RGS1
CLU
dendritic.cell.type.1
macrophage_a
macrophage_c
activated.dendritic.cell
macrophage_d
macrophage_b
dendritic.cell.type.2
plasmacytoid.dendritic.cell
Identity
Expression Level
B
macrophage_a
macrophage_c
macrophage_d
macrophage_b
Identity
CCL18
FCER1G
C1QA
GPNMB
LYZ
CD163
CD14
MRC1
CSF1R
MARCO
SPP1
ITGAM
CD68
Features
25
50
75
Average Expression
1.0
0.5
0.0
-0.5
-1.0
C
D
macrophage_a
CCL21
FCER1G
C1QA
macrophage_b
LYZ
CLEC4E
GPNMB
macrophage_c
CD14
MRC1
CSF1R
macrophage_d
SPP1
MARCO
FN1
umap_1
umap_2

Fig.3

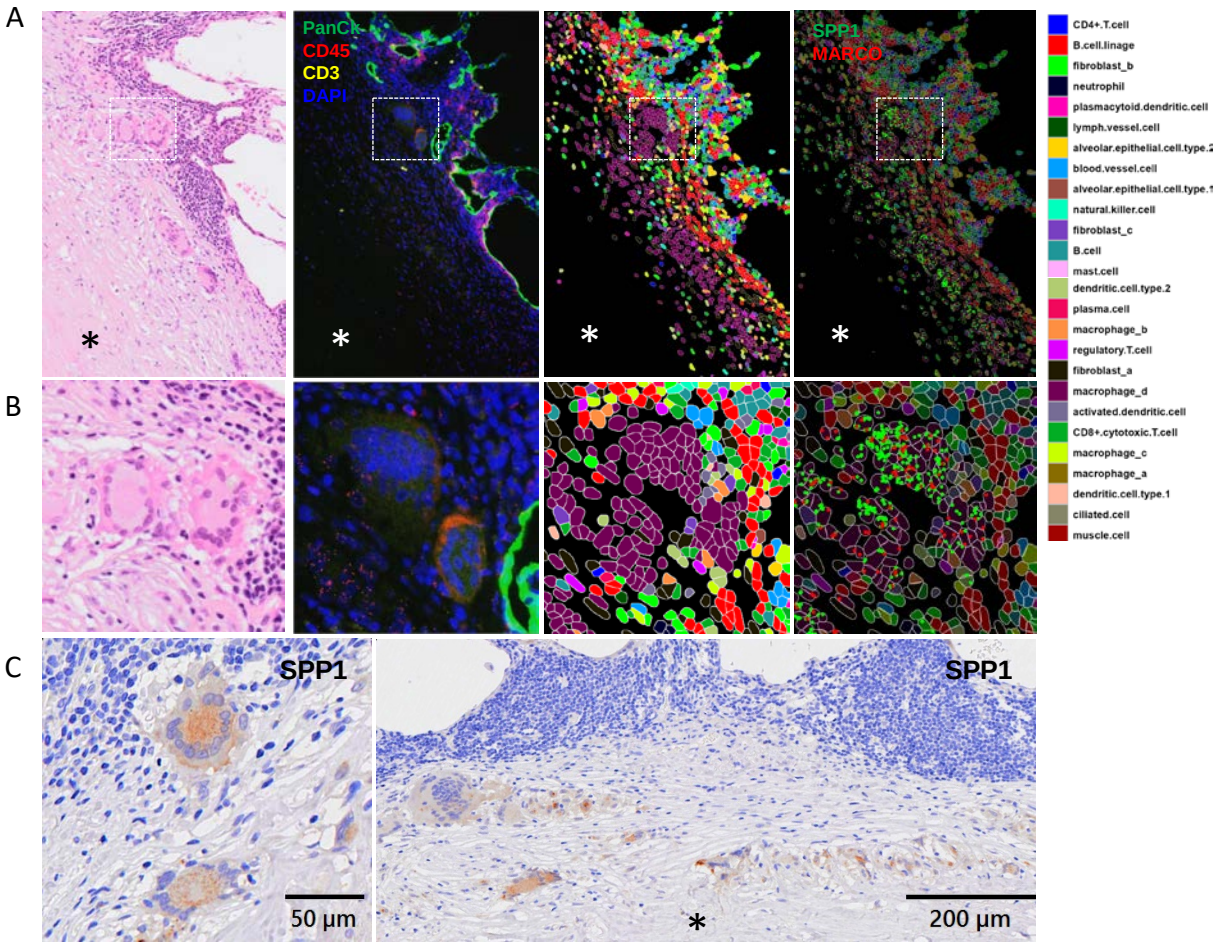
A
PanCk
CD45
CD3
DAPI
SPP1
MARCO
B
C
SPP1
SPP1
50 μm
200 μm
CD4+.T.cell
B.cell.linage
fibroblast_b
neutrophil
plasmacytoid.dendritic.cell
lymph.vessel.cell
alveolar.epithelial.cell.type.2
blood.vessel.cell
alveolar.epithelial.cell.type.1
natural.killer.cell
fibroblast_c
B.cell
mast.cell
dendritic.cell.type.2
plasma.cell
macrophage_b
regulatory.T.cell
fibroblast_a
macrophage_d
activated.dendritic.cell
CD8+.cytotoxic.T.cell
macrophage_c
macrophage_a
dendritic.cell.type.1
ciliated.cell
muscle.cell

Fig.4

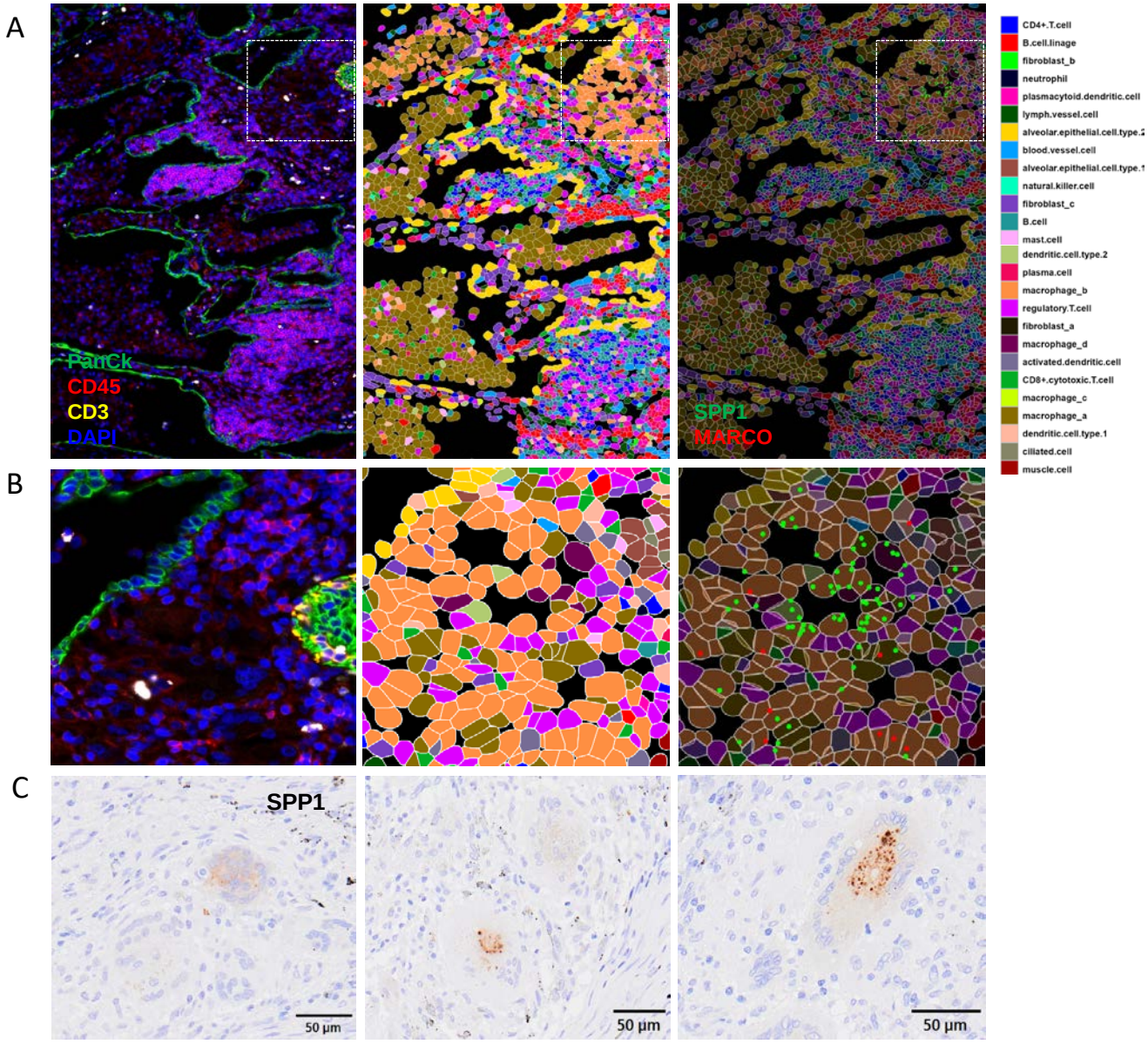
A
PanCk
CD45
CD3
DAPI
SPP1
MARCO
CD4+.T.cell
B.cell.linage
fibroblast_b
neutrophil
plasmacytoid.dendritic.cell
lymph.vessel.cell
alveolar.epithelial.cell.type.2
blood.vessel.cell
alveolar.epithelial.cell.type.1
natural.killer.cell
fibroblast_c
B.cell
mast.cell
dendritic.cell.type.2
plasma.cell
macrophage_b
regulatory.T.cell
fibroblast_a
macrophage_d
activated.dendritic.cell
CD8+.cytotoxic.T.cell
macrophage_c
macrophage_a
dendritic.cell.type.1
ciliated.cell
muscle.cell
B
C
SPP1
50 µm
50 µm
50 µm

Fig.5

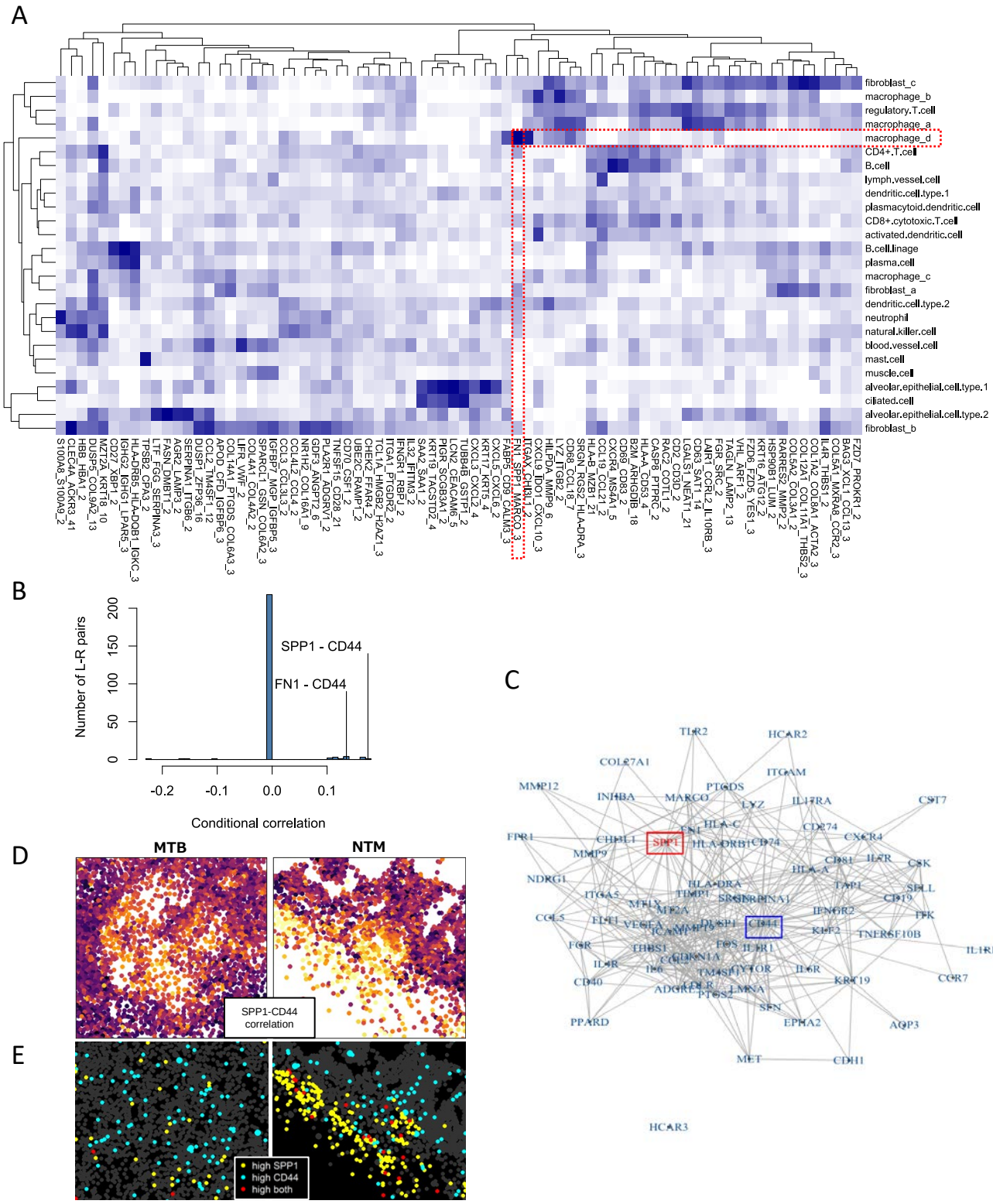
A
fibroblast_c
macrophage_b
regulatory.T.cell
macrophage_a
macrophage_d
CD4+.T.cell
B.cell
lymph.vessel.cell
dendritic.cell.type.1
plasmacytoid.dendritic.cell
CD8+.cytotoxic.T.cell
activated.dendritic.cell
B.cell.linage
plasma.cell
macrophage_c
fibroblast_a
dendritic.cell.type.2
neutrophil
natural.killer.cell
blood.vessel.cell
mast.cell
muscle.cell
alveolar.epithelial.cell.type.1
ciliated.cell
alveolar.epithelial.cell.type.2
fibroblast_b
B
Number of L-R pairs
SPP1 - CD44
FN1 - CD44
Conditional correlation
C
D
MTB
NTM
SPP1-CD44 correlation
E
high SPP1
high CD44
high both

Fig.6

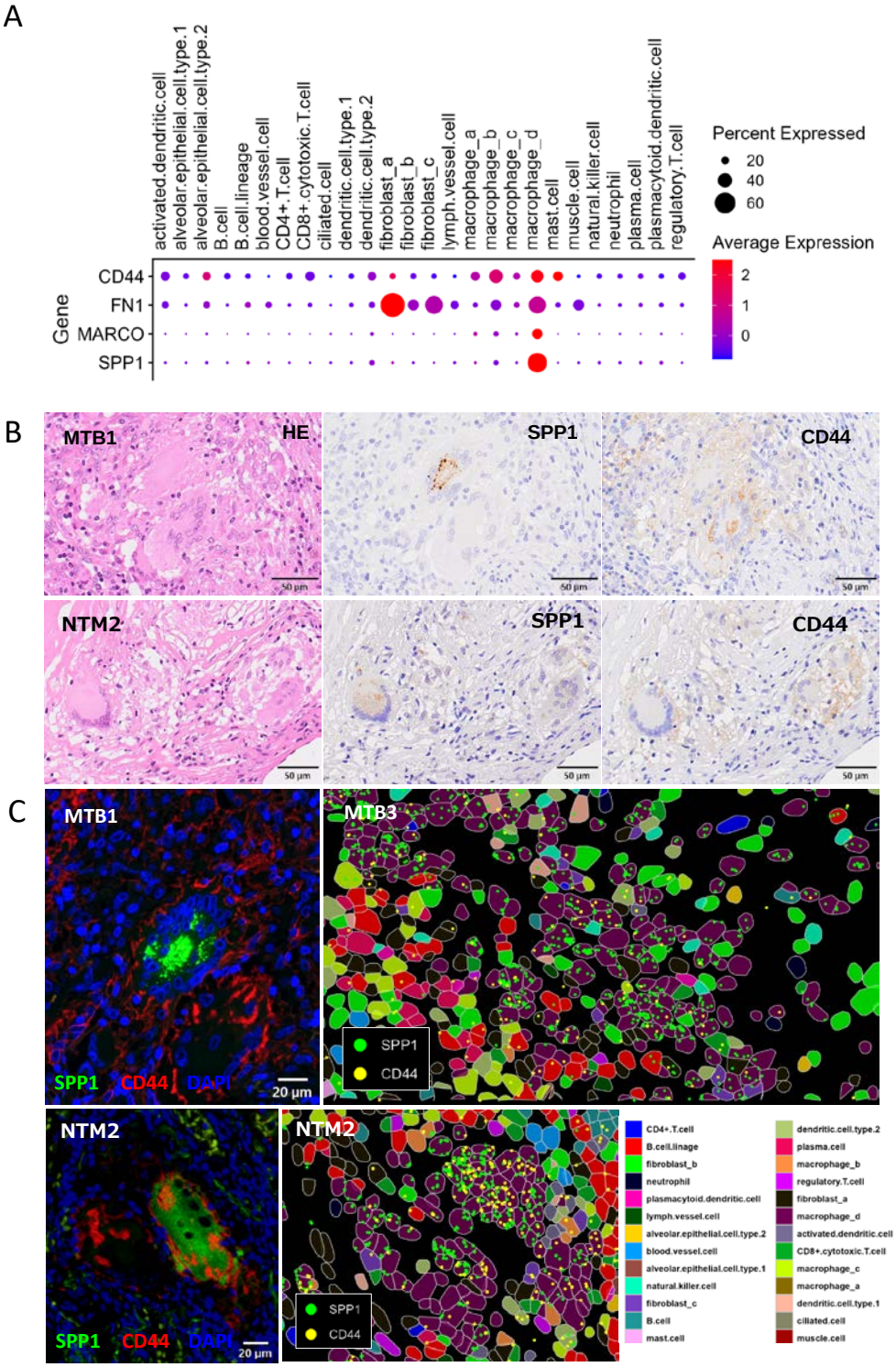
A
activated.dendritic.cell
alveolar.epithelial.cell.type.1
alveolar.epithelial.cell.type.2
B.cell
B.cell.lineage
blood.vessel.cell
CD4+.T.cell
CD8+.cytotoxic.T.cell
ciliated.cell
dendritic.cell.type.1
dendritic.cell.type.2
fibroblast_a
fibroblast_b
fibroblast_c
lymph.vessel.cell
macrophage_a
macrophage_b
macrophage_c
macrophage_d
mast.cell
muscle.cell
natural.killer.cell
neutrophil
plasma.cell
plasmacytoid.dendritic.cell
regulatory.T.cell
Gene
CD44
FN1
MARCO
SPP1
Percent Expressed
20
40
60
Average Expression
2
1
0
B
MTB1
HE
SPP1
CD44
NTM2
SPP1
CD44
50 μm
C
MTB1
SPP1
CD44
DAPI
20 μm
MTB3
SPP1
CD44
NTM2
SPP1
CD44
DAPI
20 μm
NTM2
SPP1
CD44
CD4+.T.cell
B.cell.lineage
fibroblast_b
neutrophil
plasmacytoid.dendritic.cell
lymph.vessel.cell
alveolar.epithelial.cell.type.2
blood.vessel.cell
alveolar.epithelial.cell.type.1
natural.killer.cell
fibroblast_c
B.cell
mast.cell
dendritic.cell.type.2
plasma.cell
macrophage_b
regulatory.T.cell
fibroblast_a
macrophage_d
activated.dendritic.cell
CD8+.cytotoxic.T.cell
macrophage_c
macrophage_a
dendritic.cell.type.1
ciliated.cell
muscle.cell

Fig.7

A

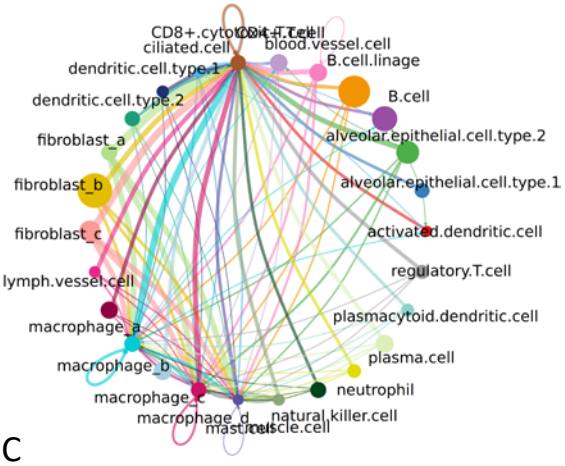

B

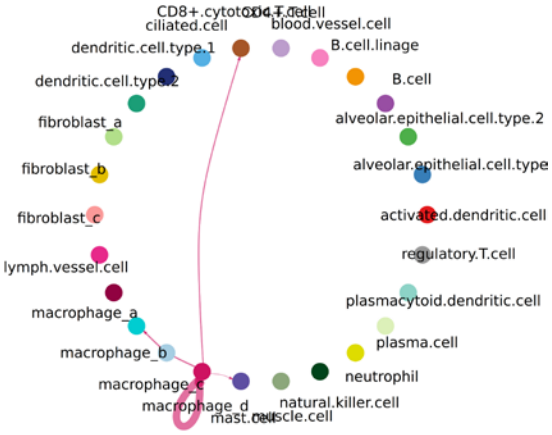

C

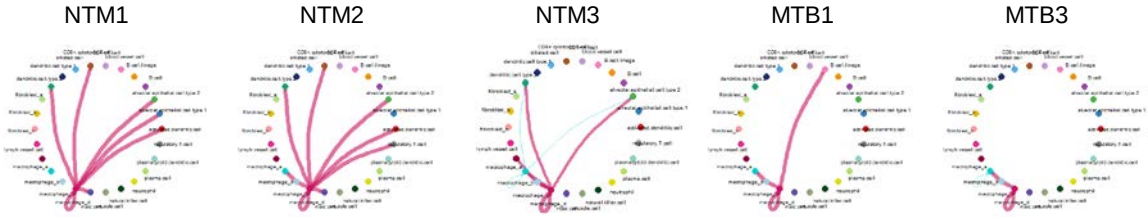

D

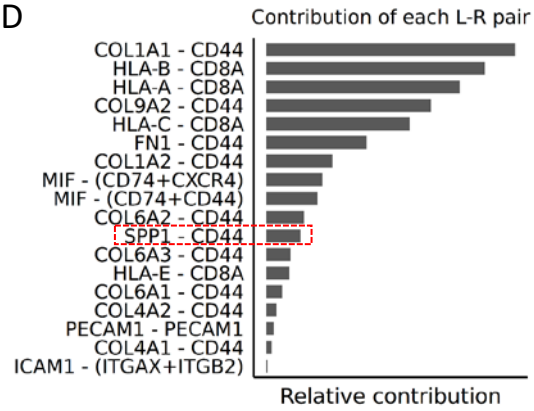

E

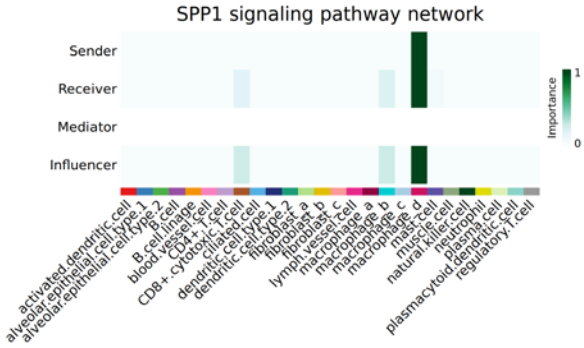

F

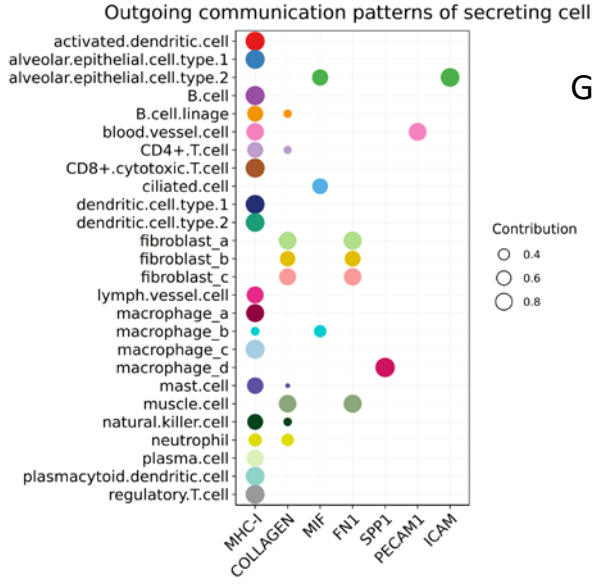

G

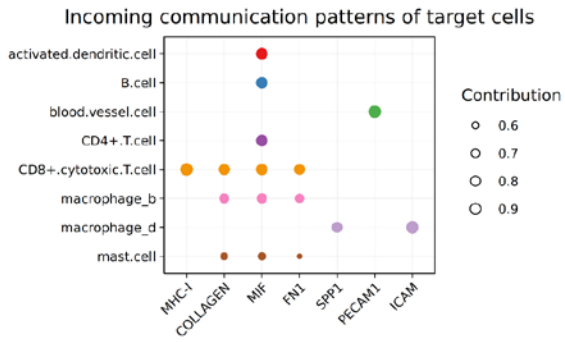

Fig.8

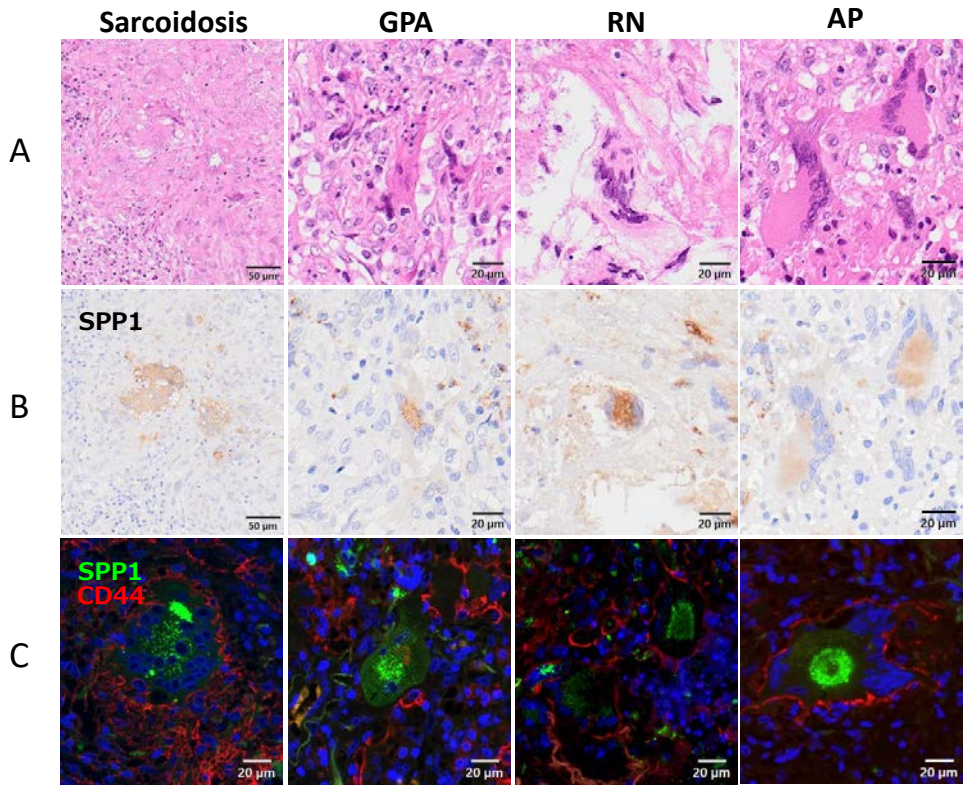

Supplementary Infomation

Identification of SPP1-positive macrophages by single-cell spatial analysis in human lung tissues with mycobacterial infection

Harutaka Katano, Akira Hebisawa, Yuko Sato, Yoshihiko Hoshino

The PDF file includes:

Figs. S1 to S11

Tables S1 to S4

Other Supplementary Material for this manuscript includes the following:

marker_heatmap_nb_clus_4.csv

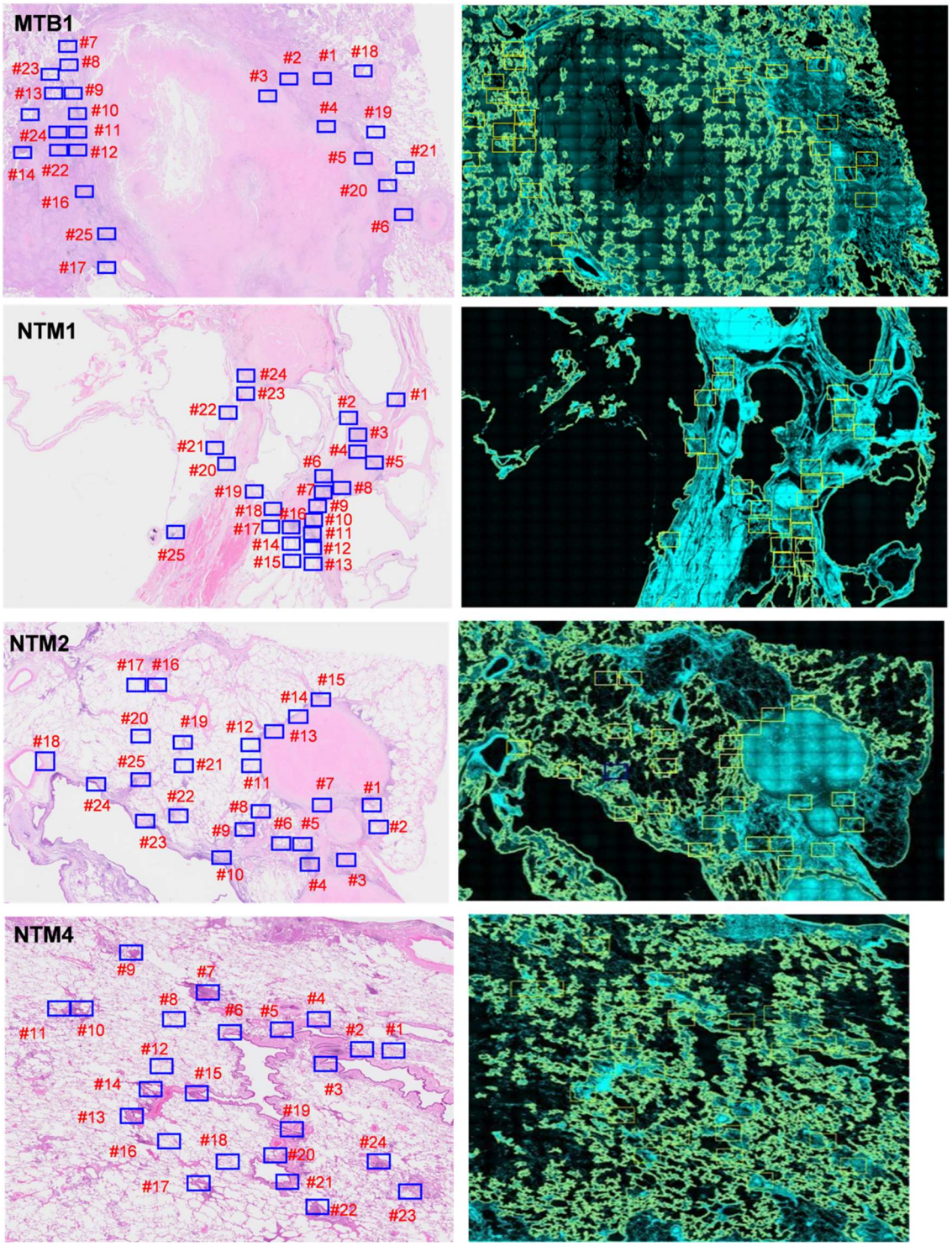

Supplementary Fig.S1a: CosMx FOV placements.

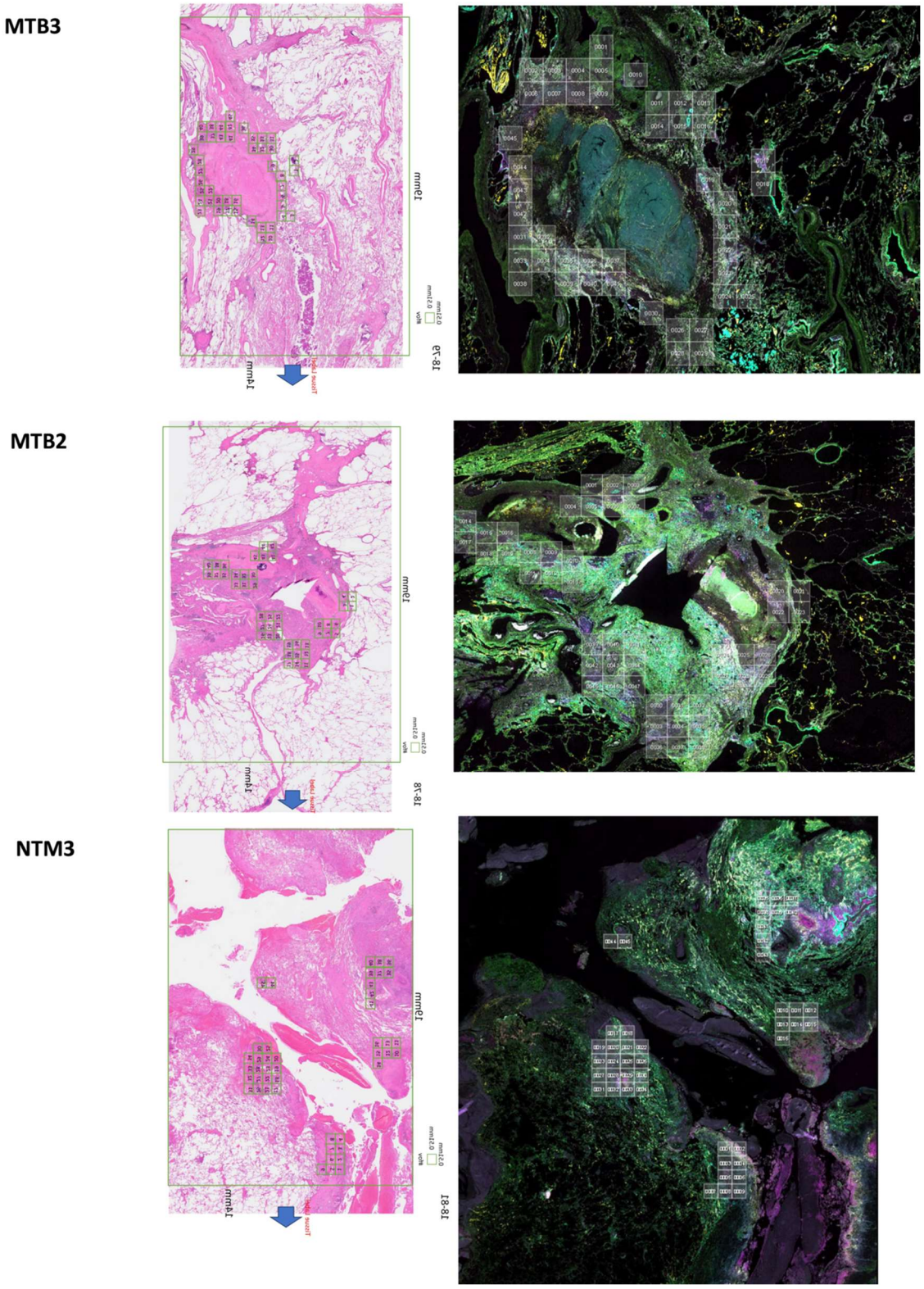

Supplementary Fig.S1b: CosMx FOV placements.

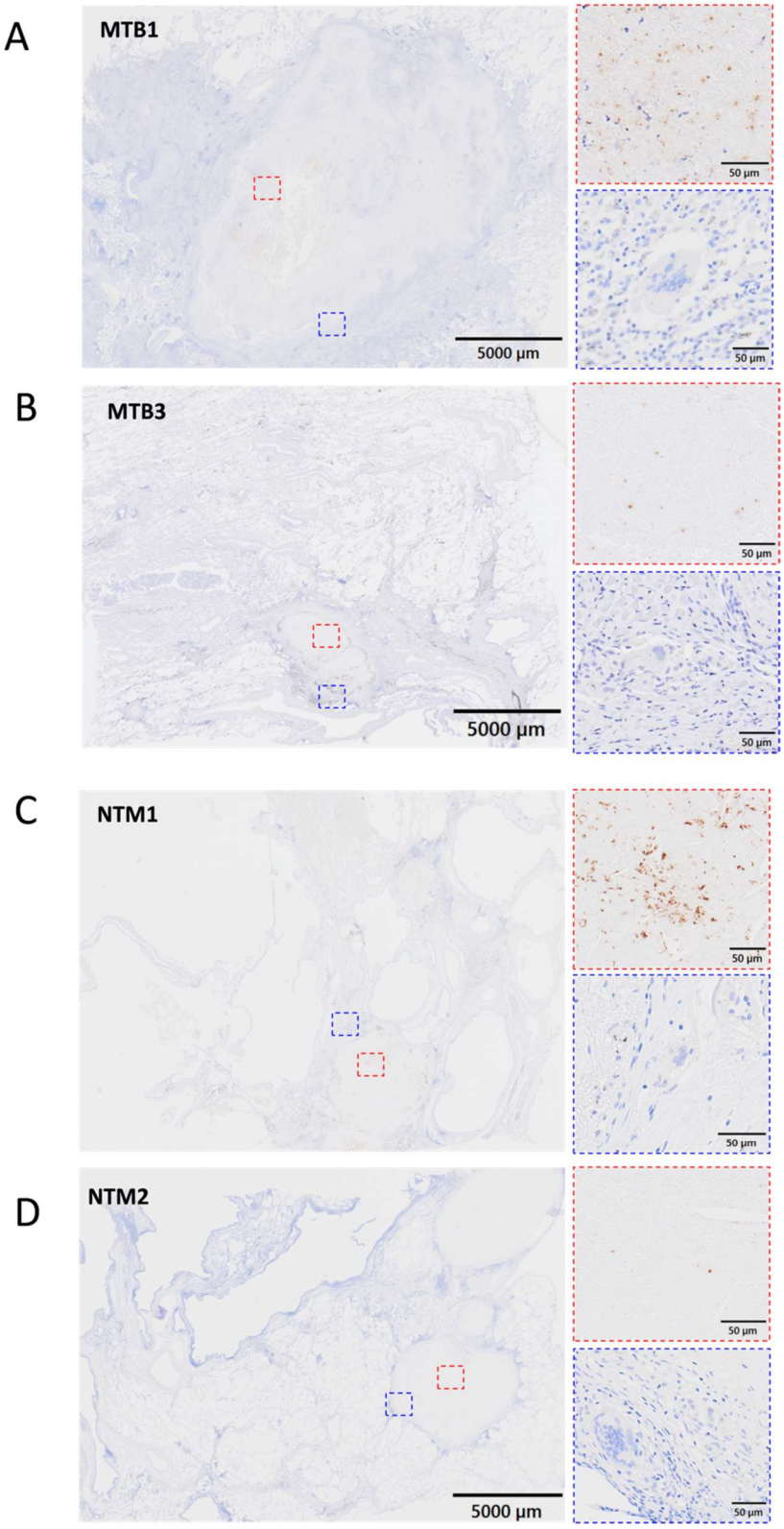

Supplementary Fig. S2: Immunohistochemistry for BCG. Blue and red boxes (right panels) show the enlarged images of left panels.

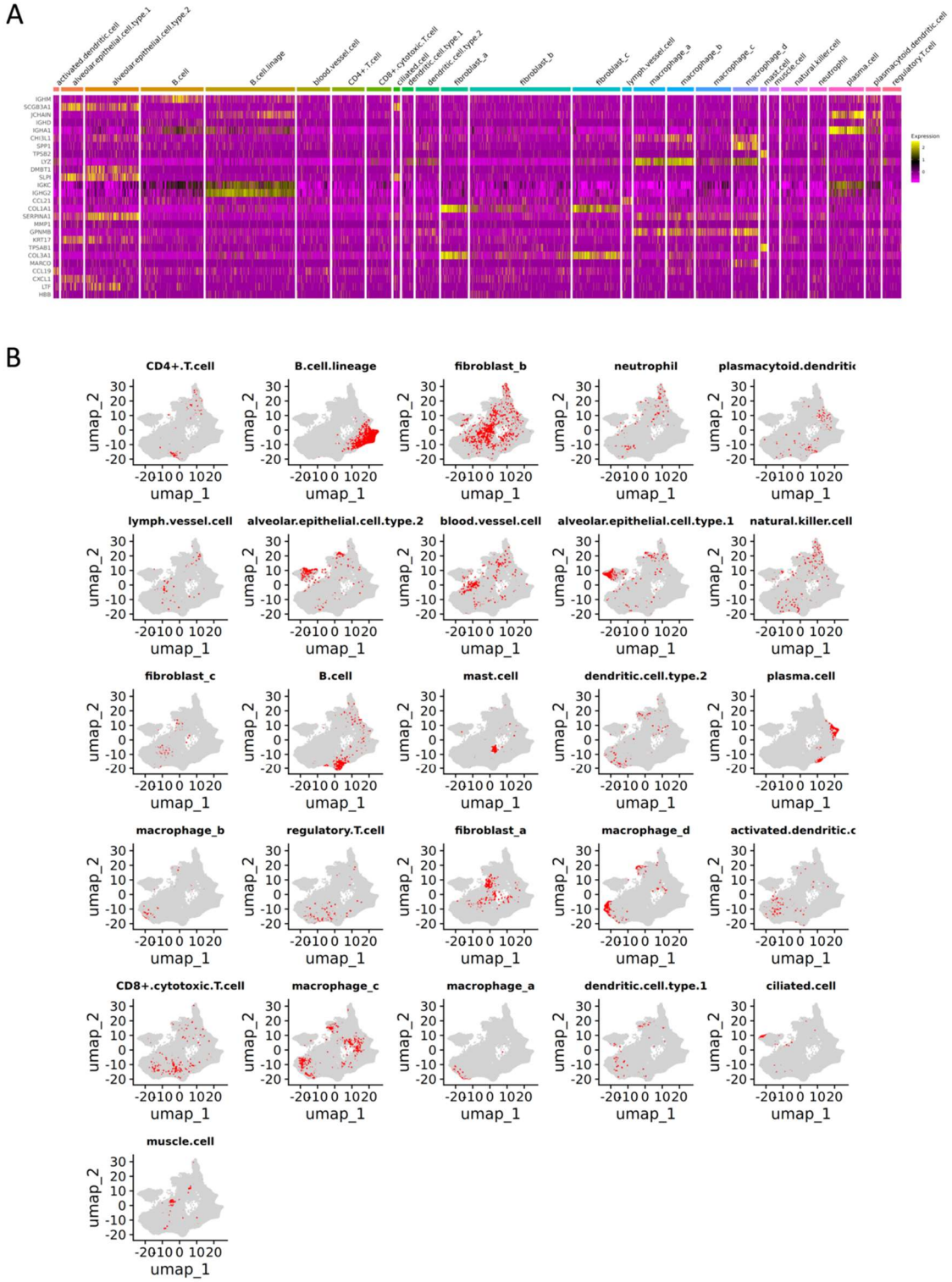

Supplementary Fig. S3: Single cell analysis of CosMx™ in mycobacterium-infected tissues. A. Heatmap showing gene expression and cell types based on single-cell data from CosMx™. B. UMAP visualization of cell types, with each cell type displayed in a red color.

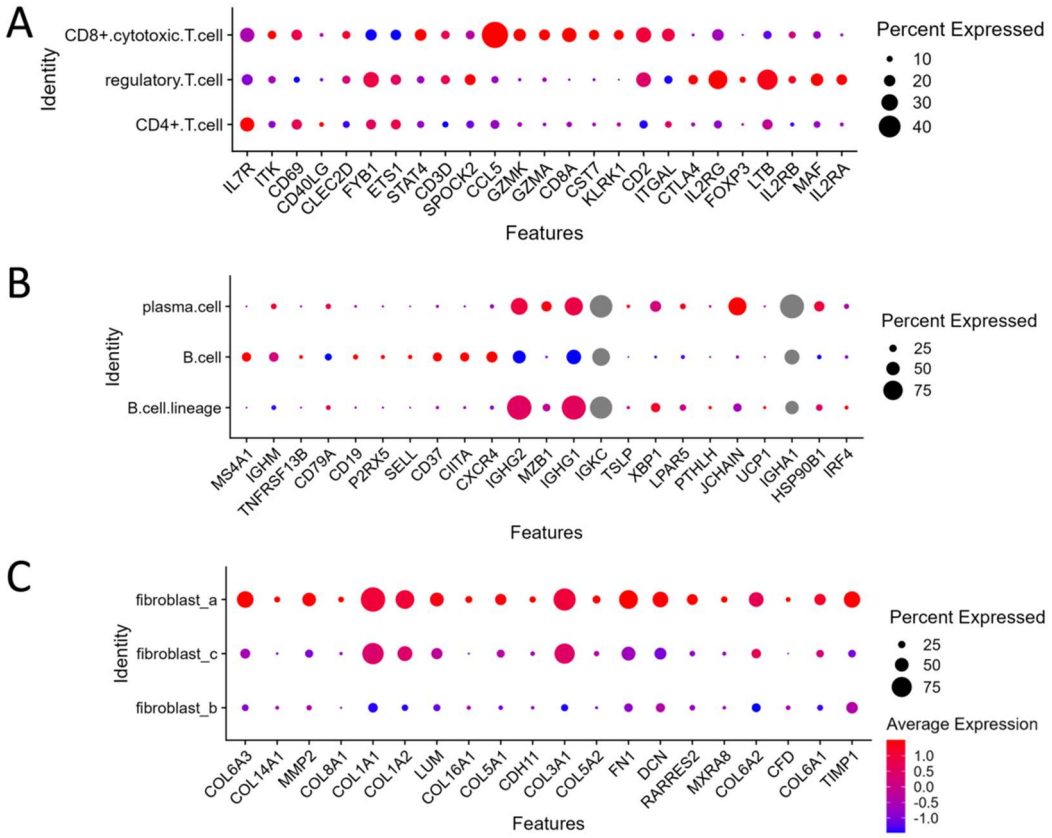

Supplementary Fig. S4: Dot plot showing gene expression in subtypes of T cells, B cells, and fibroblasts in single-cell analysis of CosMx™ in mycobacterium-infected tissues. A. Dot plot displaying gene expression in three T cell subtypes. B. Dot plot displaying gene expression in three B cell subtypes. C. Dot plot displaying gene expression in three fibroblast subtypes.

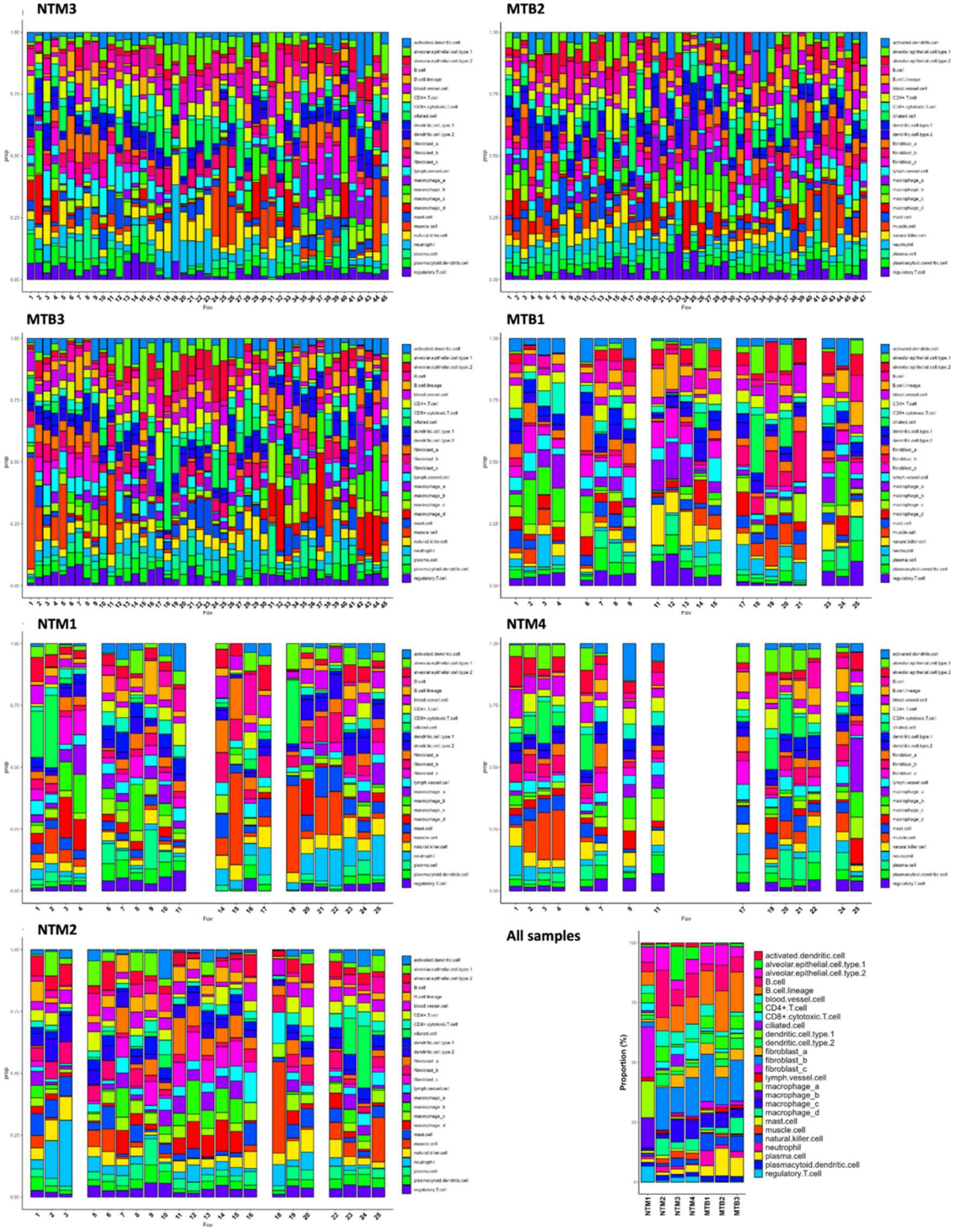

Supplementary Fig. S5: Populations of cell types in each tissue. Distribution of cell type across fovs in each slide and all samples (the right bottom panel).

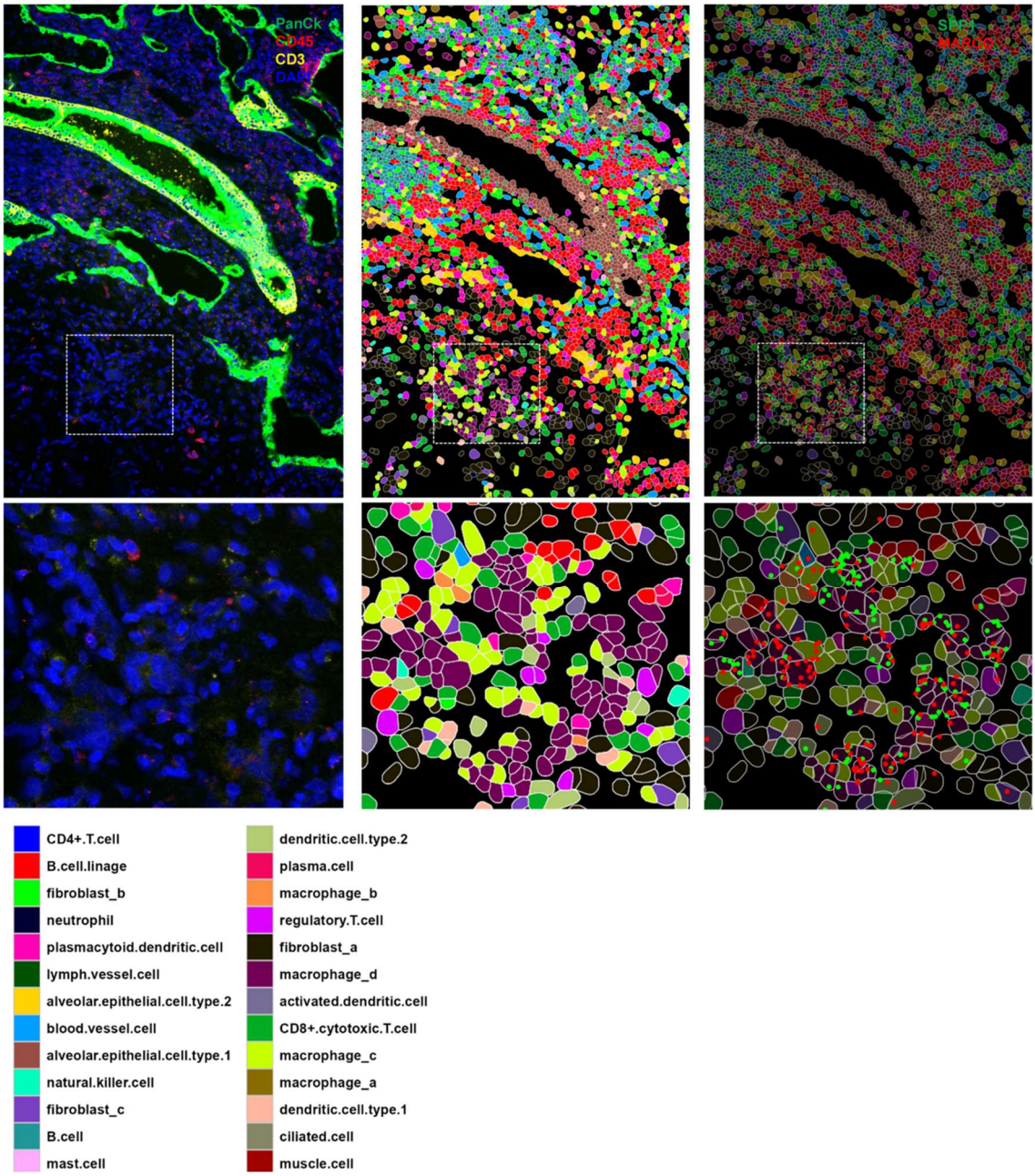

Supplementary Fig. S6a: CosMx™ spatial images of SPP1 and MARCO expression in macrophage_d within MAC+ tissue (NTM2 fov9). Upper panels: Macrophage_d in the interstitial region expressing SPP1 and MARCO. Lower panels: Enlarged view of upper panel. Colors indicating cell types are shown in the bottom panel.

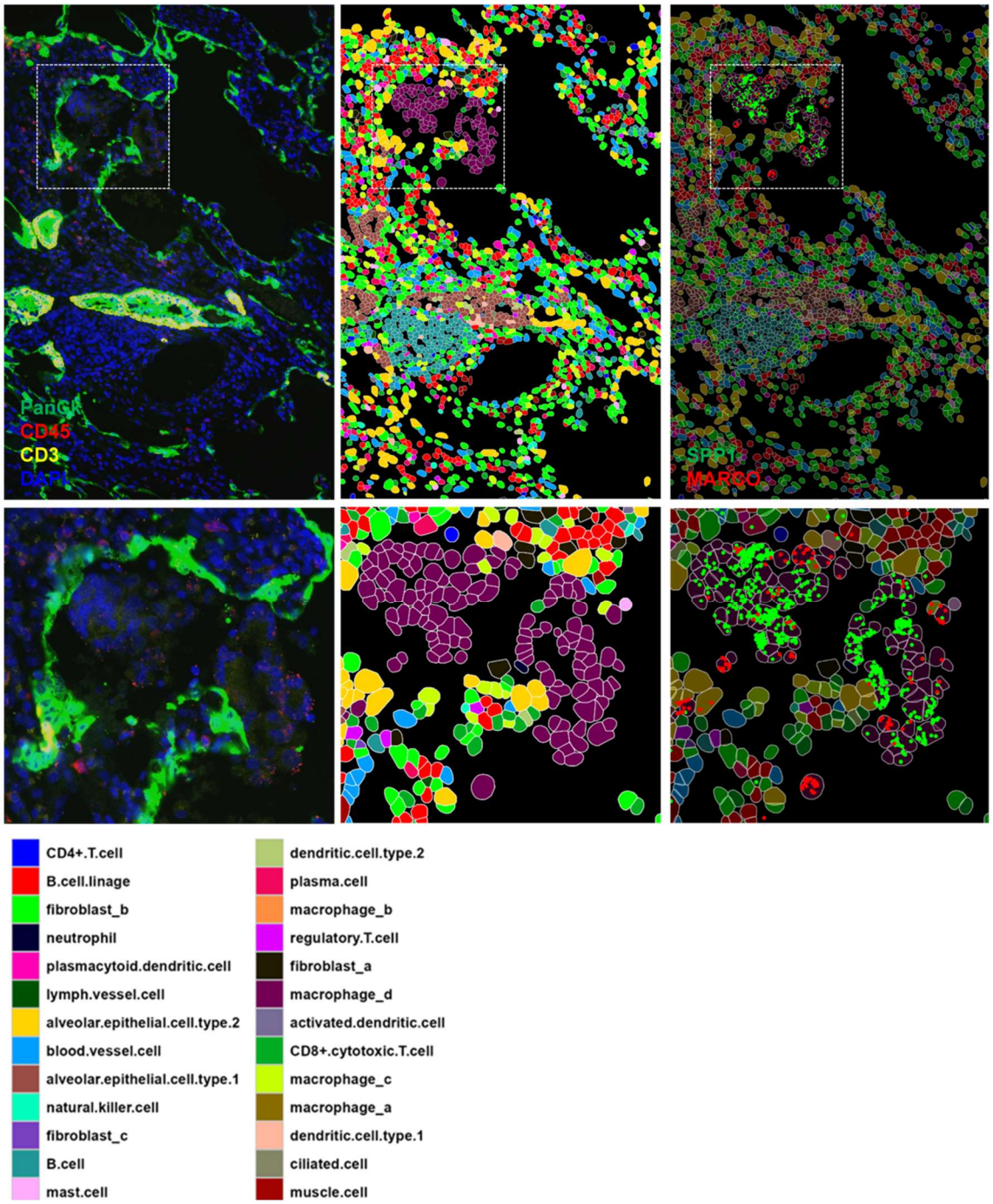

Supplementary Fig. S6b: CosMx™ spatial images of SPP1 and MARCO expression in macrophage_d within MAC+ tissue (NTM2 fov8). Upper panels: Macrophage_d in the interstitial region expressing SPP1 and MARCO. Lower panels: Enlarged view of upper panel. Colors indicating cell types are shown in the bottom panel.

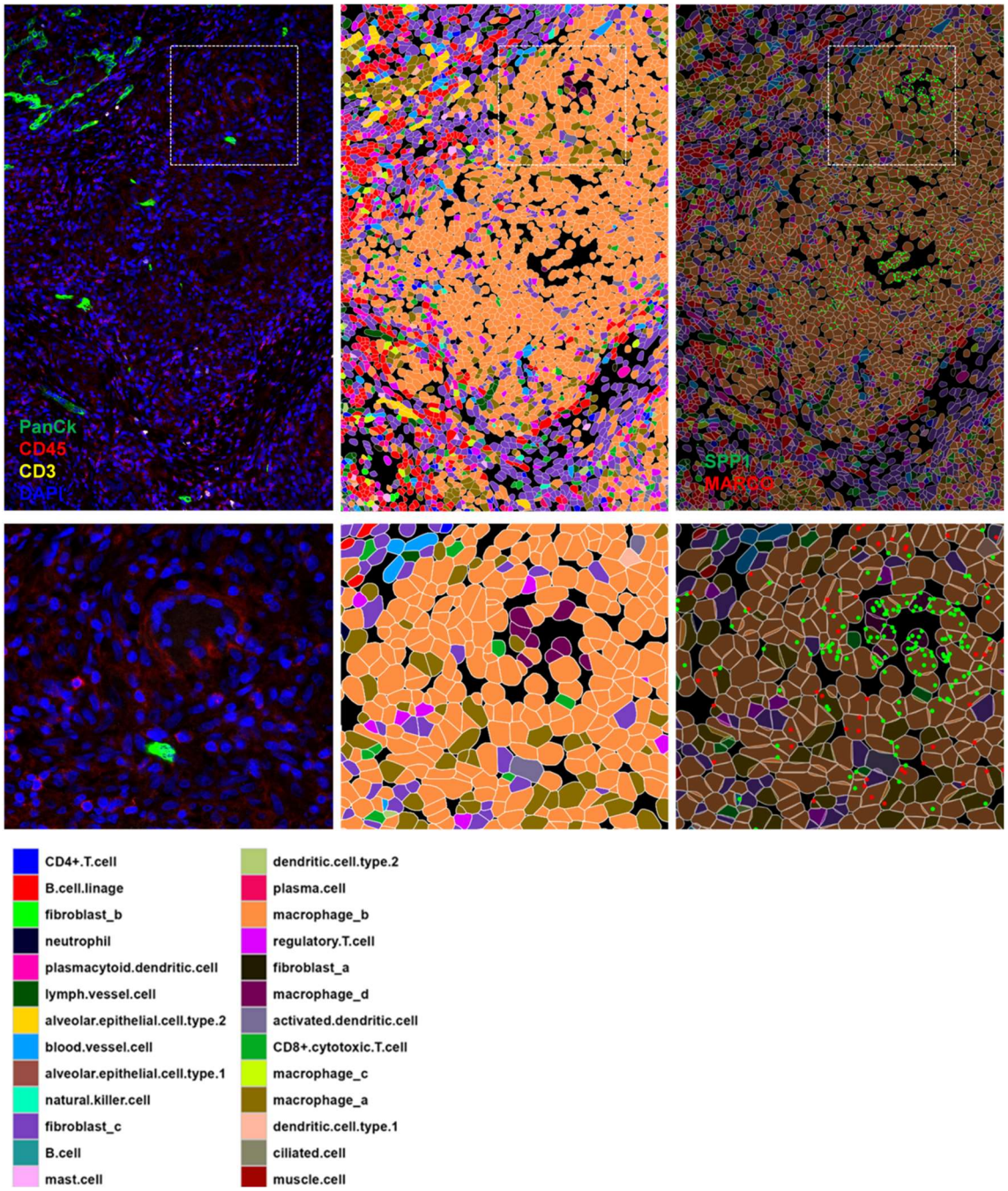

Supplementary Fig. S6c: CosMx™ spatial images of SPP1 and MARCO expression in macrophage_d within MTB+ tissue (MTB1 fov24). Upper panels: Macrophage_d in the interstitial region expressing SPP1 and MARCO. Lower panels: Enlarged view of upper panel. Colors indicating cell types are shown in the bottom panel.

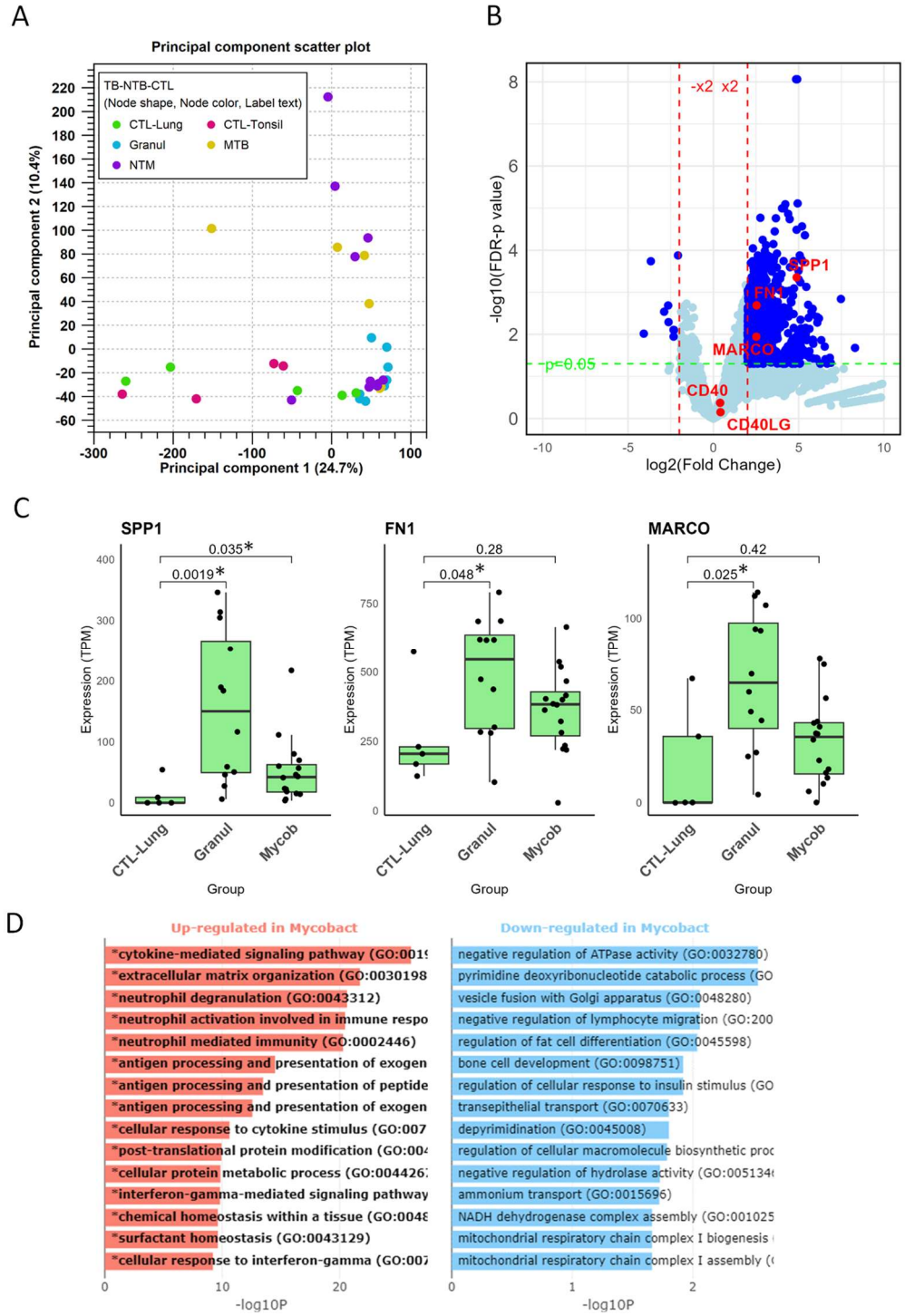

Supplementary Fig. S7: RNAseq Results for granulomatous diseases and mycobacterial infection. A. Principal component analysis (PCA) of RNA-seq data from 37 samples. B. Volcano plot comparing all granulomatous diseases (mycobacterial infections and granulomatous diseases other than mycobacterial infections) to control groups. The expression levels of SPP1, FN1, and MARCO are significantly higher in the overall granulomatous disease group. C. Box plot showing SPP1, FN1, and MARCO expression in control lung (CTL-Lung, n=5), granulomatous diseases other

than mycobacterial infection (Granul, n=12), and the mycobacterial infection group (MTB+NTM, Mycob, n=16). Transcripts per million (TPM) values for each gene are plotted. P-values are displayed on comparison lines , with asterisks (*) indicating significant differences (Mann-Whitney test). D. Gene Ontology (GO) analysis comparing mycobacterial infection tissues to control lungs, with upregulated pathways listed in the left panel.

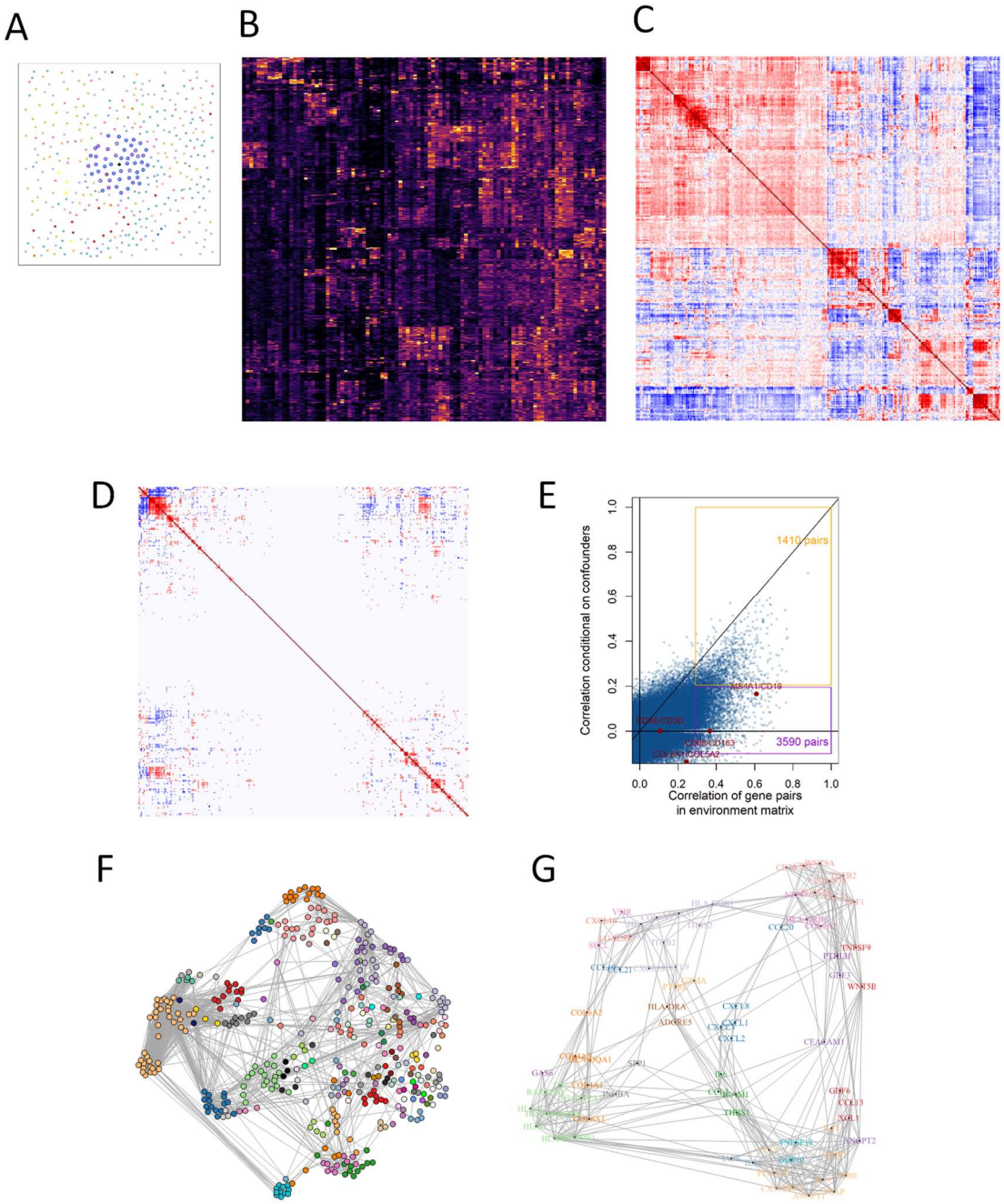

Supplementary Fig. S8: InSituCor analysis in MTB and NTM samples. A. Example of a cell's nearest neighbors, used to define its "environment expression" profile. B. Subset of the environment expression matrix. C. Raw correlation matrix of the environment expression matrix showing near-ubiquitous correlations (subset of 300 random genes). D. Correlation matrix of the environment expression matrix (B), conditioned on the confounding matrix, over the same subset of genes as in (C). E. Raw vs. conditional correlation of environment gene expression. Selected pairs of marker genes are highlighted. F. Network representation of correlation between all genes in all modules. Genes with correlation > 0.2 are connected. G. Correlation structure of 51 ligands

assigned to modules. Edges show conditional correlations > 0.1, and color shows module membership.

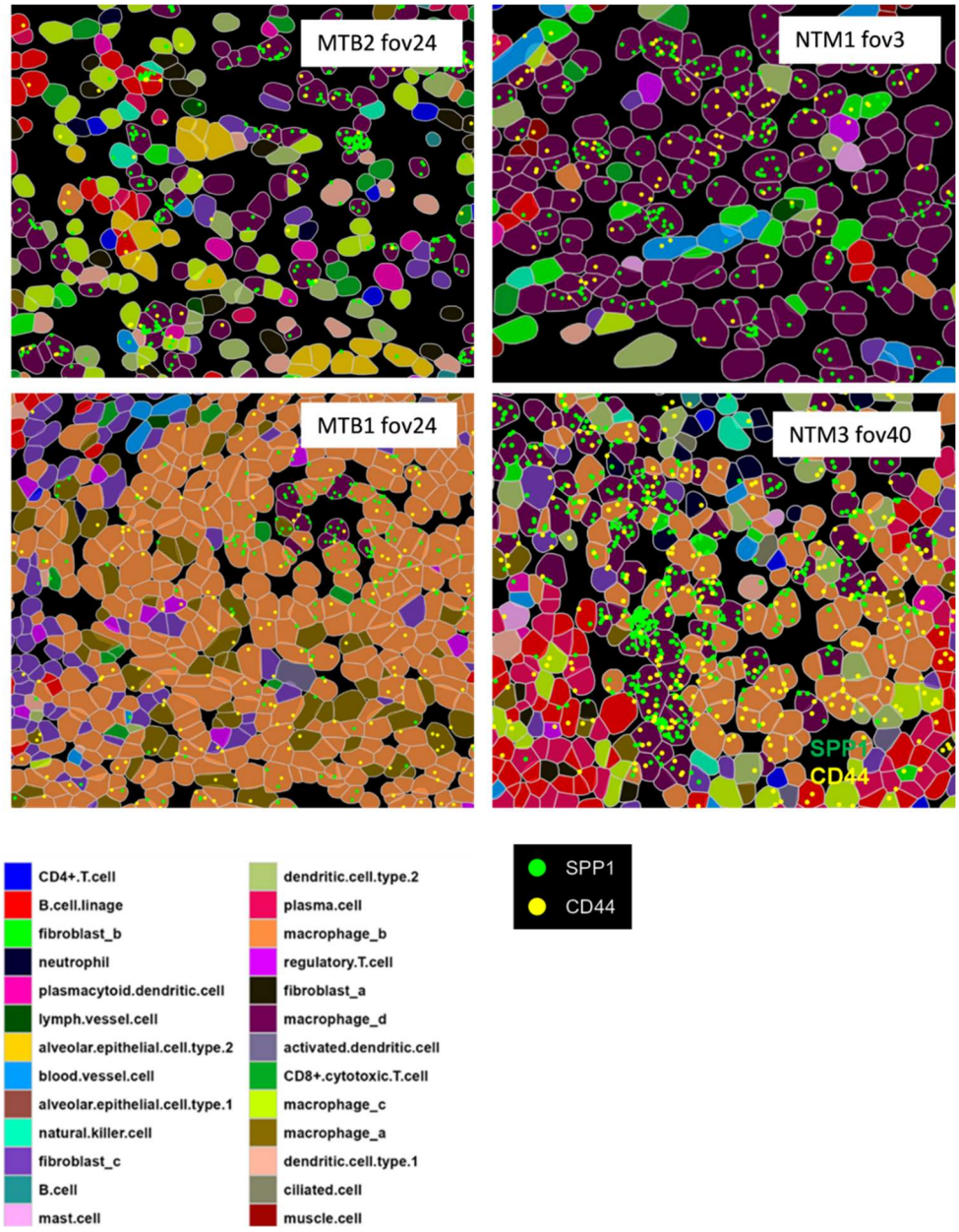

Supplementary Fig. 9. CosMx spatial images of SPP1 and CD44 expression in MTB and NTM tissues. Colors indicating cell types are shown in the bottom panel.

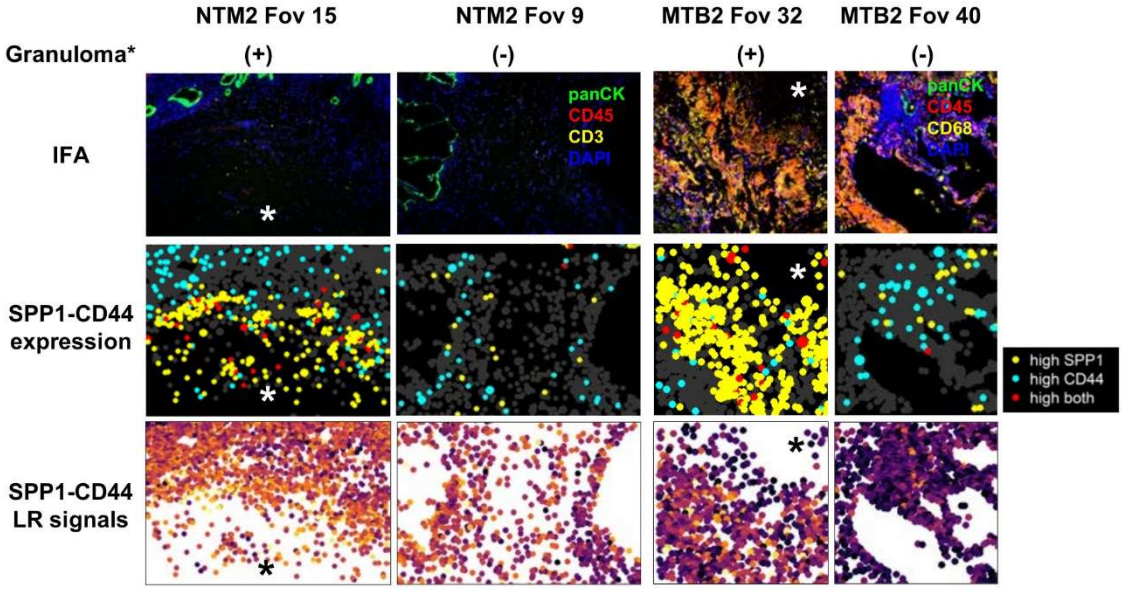

Supplementary Fig. S10. Co-expression and ligand-receptor assay in InSituCor. Immunofluorescence assay (IFA, upper panels) spatial images showing SPP1-CD44 expression (middle panels), and ligand-receptor (LR) signals of SPP1-CD44 (lower panels) in MTB and NTM tissues. In the SPP1-CD44 expression images, high expression of SPP1, CD44, and both are indicated by yellow, blue, and red dots, respectively. In the SPP1-CD44 LR signals images, yellow indicates high correlation. Spatial images from CosMx™ analysis were taken from fovs with (+) and without (-) granuloma in MTB or NTM samples. Asterisks (*) show the positions of granulomas.

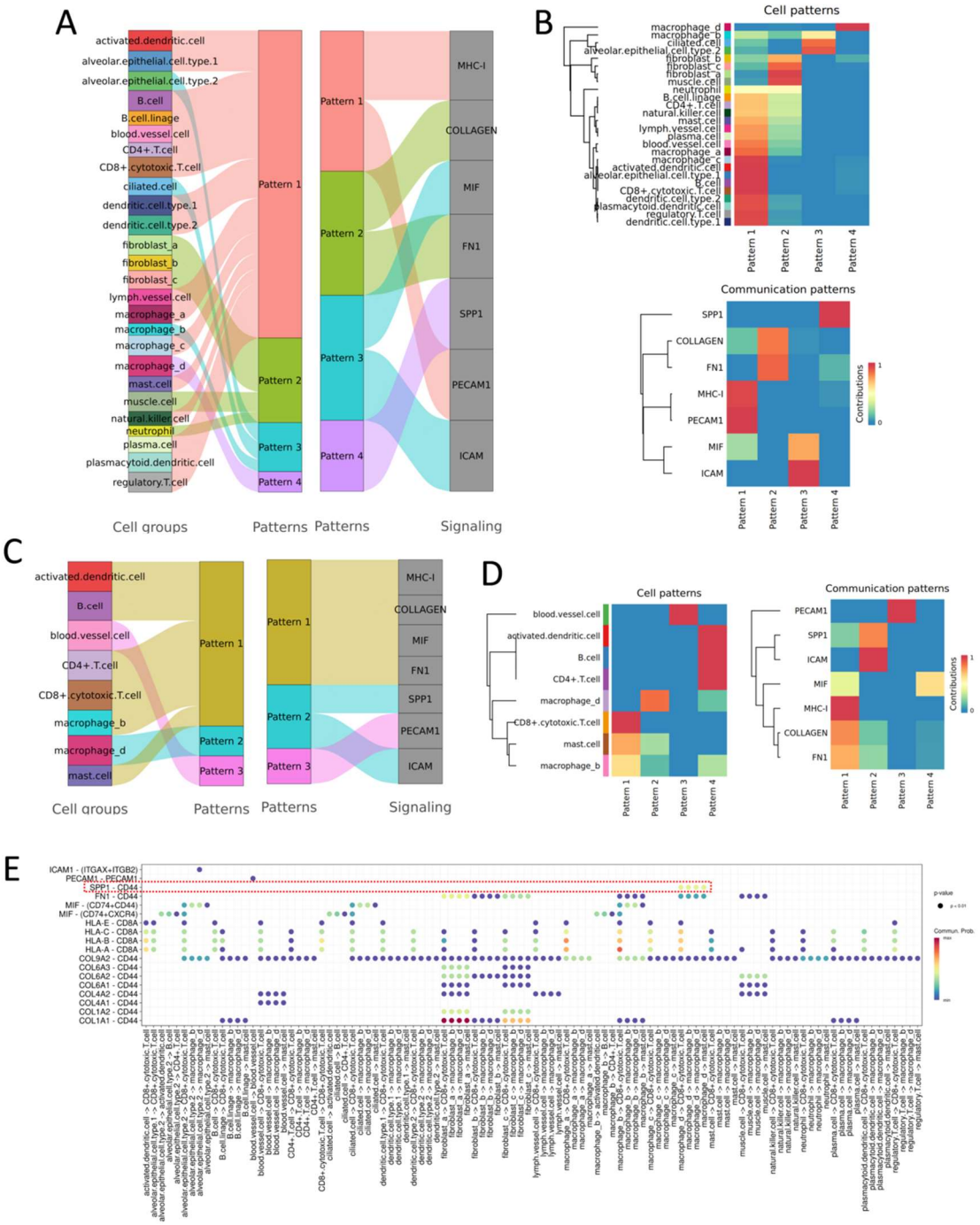

Supplementary Fig. 11: Outgoing and incoming communication patterns of secreting cells analyzed using CellChat in MTB and NTM samples. A. River plot showing cell patterns (left panel) and cell-communication patterns (right panel) for outgoing signaling pathways. B. Heatmaps displaying cell patterns (upper panel) and cell-communication patterns (lower panel) for outgoing signaling pathways. C. River plot showing cell patterns (left panel) and cell-communication patterns (right panel) for incoming signaling pathways. D. Heatmaps displaying cell patterns (upper panel) and cell-communication patterns (lower panel) for incoming signaling pathways. E. Dot

plots illustrating the incoming and outgoing interaction strength of each cell-cell communication across all ligand-receptor interactions. The SPP1-CD44 signaling pathway is highlighted with a red dashed box.

Supplementary Table S1: patient and sample list. AP: Aspergillus pneumonia, Aspi P: aspiration pneumonia, BCG: Bacille Calmette-Guerin, CTL: control, FFPE: formalin-fixed paraffin-embedded sample, GPA: granulomatosis with polyangiitis, IHC: immunohistochemistry, MAC: mycobacterium avium intracellulae complex, MTB: mycobacterium tuberculosis, NTM: non tuberculosis mycobacterium infection, ND: no data, RN: rheumatoid nodule, SA: sarcoidosis.

ID	Age	Gender	Group	Clinical diagnosis	BCG-IHC in FFPE	Real-time PCR in FFPE	CosMx
MTB1	49	M	MTB	MTB	+	MTB	MTB1
MTB2	70	M	MTB	MTB	+	MTB	MTB2
MTB3	64	M	MTB	MTB	+	MTB	MTB3
MTB4	38	M	MTB	MTB	-	MTB	
MTB5	49	M	MTB	MTB	-	-	
MTB6	49	M	MTB	MTB	-	MTB	
NTM1	71	M	NTM	NTM	+	MAC	NTM1
NTM2	56	F	NTM	NTM	+	MAC	NTM2
NTM3	63	F	NTM	NTM	+	MAC	NTM3
NTM4	51	F	NTM	NTM	-	-	NTM4
NTM5	51	F	NTM	NTM	-	-	
NTM6	51	F	NTM	NTM	+	*M. kansasii*	
NTM7	66	F	NTM	NTM	+	MAC	
NTM8	66	F	NTM	NTM	+	MAC	
NTM9	73	M	NTM	NTM	-	MAC	
NTM10	68	F	NTM	NTM	-	-	
Ctl-Lung1	62	F	CTL-Lung	Lung cancer (control)	-	-	
Ctl-Lung2	63	M	CTL-Lung	Lung cancer (control)	-	-	
Ctl-Lung3	70	M	CTL-Lung	Lung cancer (control)	-	-	
Ctl-Lung4	80	M	CTL-Lung	Lung cancer (control)	-	-	
Ctl-Lung5	54	M	CTL-Lung	Lung cancer (control)	-	-	
Ctl-Tonsil1	ND	ND	CTL-Tonsil	tonsillitis (control)	-	-	
Ctl-Tonsil2	ND	ND	CTL-Tonsil	tonsillitis (control)	-	-	
Ctl-Tonsil3	ND	ND	CTL-Tonsil	tonsillitis (control)	-	-	
Ctl-Tonsil4	ND	ND	CTL-Tonsil	tonsillitis (control)	-	-	
Granulo1	70	M	Granulo	RN	-	-	
Granulo2	77	M	Granulo	RN	-	-	
Granulo3	50	M	Granulo	AP	-	-	
Granulo4	52	M	Granulo	AP	-	-	
Granulo5	69	F	Granulo	AP	-	-	
Granulo6	58	F	Granulo	GPA	-	-	
Granulo7	71	M	Granulo	GPA	-	-	
Granulo8	77	F	Granulo	GPA	-	-	
Granulo9	56	F	Granulo	SA	-	-	
Granulo10	37	F	Granulo	SA	-	-	
Granulo11	37	M	Granulo	SA	-	-	
Granulo12	62	M	Granulo	Aspi P	-	-	

Supplementary Table S2: **Gene list of the 'CosMx Human Universal Cell Characterization' panel.**

AATK	ABL1	ABL2	ACE	ACE2	ACKR1	ACKR3	ACKR4	ACTA2	ACTG2
ACVR1	ACVR1B	ACVR2A	ACVRL1	ADGRA2	ADGRA3	ADGRB2	ADGRB3	ADGRD1	ADGRE1
ADGRE2	ADGRE5	ADGRF1	ADGRF3	ADGRF4	ADGRF5	ADGRG1	ADGRG2	ADGRG3	ADGRG5
ADGRG6	ADGRL1	ADGRL2	ADGRL4	ADGRV1	ADIPOQ	ADIRF	ADM2	ADORA2A	AGR2
AHI1	AHR	AKT1	ALCAM	ANGPT1	ANGPT2	ANGPT4	ANGPTL1	ANXA1	ANXA2
ANXA4	APOA1	APOB	APOD	APP	AQP3	AR	AREG	ARF1	ARG1
ARHGDIB	ARTN	ATF3	ATG10	ATG12	ATG5	ATM	ATR	AXL	AZGP1
AZU1	B2M	B3GNT7	BAG3	BATF3	BAX	BCL2	BCL2L1	BECN1	BEST1
BGN	BID	BIRC5	BMP1	BMP2	BMP3	BMP4	BMP5	BMP6	BMP7
BMPR1A	BMPR2	BMX	BRCA1	BST1	BST2	BTG1	BTK	C11orf96	C1QA
C1QB	C1QC	C5AR2	C9orf16	CALB1	CALD1	CALM1	CALM2	CALM3	CAMP
CASP3	CASP8	CASR	CAV1	CCL11	CCL13	CCL15	CCL18	CCL19	CCL2
CCL20	CCL21	CCL23	CCL26	CCL28	CCL3	CCL3L3	CCL4	CCL4L2	CCL5
CCL7	CCL8	CCND1	CCR1	CCR10	CCR2	CCR5	CCR7	CCRL2	CD14
CD163	CD164	CD19	CD2	CD209	CD24	CD27	CD274	CD276	CD28
CD300A	CD33	CD34	CD36	CD37	CD38	CD3D	CD3E	CD3G	CD4
CD40	CD40LG	CD44	CD47	CD48	CD52	CD53	CD55	CD58	CD59
CD5L	CD63	CD68	CD69	CD70	CD74	CD79A	CD80	CD81	CD83
CD84	CD86	CD8A	CD8B	CD9	CDH1	CDH11	CDH5	CDKN1A	CDKN3
CEACAM1	CEACAM6	CELSR1	CELSR2	CENPF	CFD	CFLAR	CHEK1	CHEK2	CHGA
CHI3L1	CIDEA	CIITA	CLCF1	CLDN4	CLEC10A	CLEC12A	CLEC14A	CLEC1A	CLEC2B
CLEC2D	CLEC4A	CLEC4D	CLEC4E	CLEC5A	CLEC7A	CLOCK	CLU	CMKLR1	CNTFR
COL11A1	COL12A1	COL14A1	COL15A1	COL16A1	COL17A1	COL18A1	COL1A1	COL1A2	COL21A1
COL27A1	COL3A1	COL4A1	COL4A2	COL4A5	COL5A1	COL5A2	COL5A3	COL6A1	COL6A2
COL6A3	COL8A1	COL9A1	COL9A2	COL9A3	COTL1	CPA3	CPB1	CRIP1	CRP
CRYAB	CSF1	CSF1R	CSF2	CSF2RA	CSF2RB	CSF3	CSF3R	CSHL1	CSK
CST7	CTLA4	CTNNB1	CTSG	CTSW	CUZD1	CX3CL1	CX3CR1	CXCL1	CXCL10
CXCL12	CXCL14	CXCL16	CXCL17	CXCL2	CXCL3	CXCL5	CXCL6	CXCL8	CXCL9
CXCR1	CXCR2	CXCR3	CXCR4	CXCR5	CXCR6	CYP19A1	CYP1B1	CYSTM1	CYTOR
DCN	DDC	DDIT3	DDR1	DDR2	DDX58	DHRS2	DLL1	DMBT1	DNMT1
DNMT3A	DNTT	DPP4	DST	DUSP1	DUSP2	DUSP4	DUSP5	DUSP6	EFNA1
EFNA4	EFNA5	EFNB1	EFNB2	EFNB3	EGF	EGFR	EIF5A	ELANE	EMP3
ENG	ENTPD1	EOMES	EPCAM	EPHA2	EPHA3	EPHA4	EPHA7	EPHB2	EPHB3
EPHB4	EPHB6	EPOR	ERBB2	ERBB3	ESAM	ESR1	ETS1	ETV4	ETV5
EZH2	EZR	FABP4	FABP5	FAS	FASLG	FASN	FCER1G	FCGBP	FCGR3A
FCRLA	FES	FFAR2	FFAR3	FFAR4	FGF1	FGF12	FGF13	FGF18	FGF2
FGF7	FGF9	FGFR1	FGFR2	FGFR3	FGG	FGR	FKBP11	FLT1	FLT3LG
FN1	FOS	FOXF1	FOXP3	FPR1	FYB1	FYN	FZD1	FZD3	FZD4
FZD5	FZD6	FZD7	FZD8	G6PC2	G6PD	GADD45B	GAS6	GATA3	GC
GCG	GDF10	GDF15	GDF3	GDF6	GDF9	GDNF	GLUD1	GLUL	GNLY
GPBAR1	GPER1	GPNMB	GPR183	GPX1	GPX3	GSN	GSTP1	GZMA	GZMB
GZMH	GZMK	H2AZ1	H4C3	HAVCR2	HBA1	HBB	HCAR2	HCAR3	HCK
HCST	HDAC1	HDAC11	HDAC3	HDAC4	HDAC5	HGF	HIF1A	HILPDA	HLA-A
HLA-B	HLA-C	HLA-DPA1	HLA-DPB1	HLA-DQA1	HLA-DQB1	HLA-DRA	HLA-DRB1	HLA-DRB5	HLA-E
HMGB2	HMGN2	HPGDS	HSD17B2	HSD3B2	HSP90AA1	HSP90AB1	HSP90B1	HSPA1A	HSPA1B
HSPB1	HTT	IAPP	ICAM1	ICAM2	ICAM3	ICOS	ICOSLG	IDO1	IER3
IFI27	IFIH1	IFIT1	IFITM1	IFITM3	IFNA1	IFNAR1	IFNAR2	IFNB1	IFNG
IFNGR1	IFNGR2	IFNL2	IFNL3	IGF1	IGF1R	IGF2	IGF2R	IGFBP3	IGFBP5

IGFBP6	IGFBP7	IGHA1	IGHD	IGHG1	IGHG2	IGHM	IGKC	IL10	IL10RA
IL10RB	IL11	IL11RA	IL12A	IL12B	IL12RB1	IL12RB2	IL13RA1	IL15	IL15RA
IL16	IL17A	IL17B	IL17D	IL17RA	IL17RB	IL17RE	IL18	IL18R1	IL1A
IL1B	IL1R1	IL1R2	IL1RAP	IL1RL1	IL1RN	IL2	IL20	IL20RA	IL22RA1
IL23A	IL24	IL27RA	IL2RA	IL2RB	IL2RG	IL32	IL33	IL34	IL36G
IL3RA	IL4R	IL6	IL6R	IL6ST	IL7	IL7R	INHA	INHBA	INHBB
INS	INSR	IRF3	IRF4	ITGA1	ITGA2	ITGA3	ITGA5	ITGA6	ITGA9
ITGAE	ITGAL	ITGAM	ITGAV	ITGAX	ITGB1	ITGB2	ITGB4	ITGB5	ITGB6
ITGB8	ITK	ITM2A	JAG1	JAK1	JAK2	JCHAIN	JUN	JUNB	KDR
KIT	KITLG	KLF2	KLK3	KLRB1	KLRK1	KRAS	KRT1	KRT10	KRT13
KRT14	KRT15	KRT16	KRT17	KRT18	KRT19	KRT20	KRT23	KRT24	KRT4
KRT5	KRT6A	KRT6B	KRT6C	KRT7	KRT8	KRT80	KRT86	LAG3	LAIR1
LAMP2	LAMP3	LCN2	LDLR	LEFTY1	LEFTY2	LEP	LGALS1	LGALS3	LGALS3BP
LGALS9	LIF	LIFR	LINC02446	LMNA	LPAR5	LTB	LTBR	LTF	LUM
LY6D	LY75	LYN	LYZ	MAF	MALAT1	MAML2	MAP1LC3B	MAPK13	MAPK14
MARCO	MECOM	MEG3	MERTK	MET	MGP	MIF	MKI67	MMP1	MMP10
MMP12	MMP14	MMP16	MMP19	MMP2	MMP3	MMP7	MMP8	MMP9	MPO
MRC1	MRC2	MS4A1	MS4A4A	MSMB	MST1R	MT1X	MT2A	MTOR	MTRNR2L1
MX1	MXRA8	MYC	MYH11	MYL9	MZB1	MZT2A	NANOG	NCR1	NDRG1
NEAT1	NFKB1	NFKBIA	NGFR	NKG7	NLRC4	NLRC5	NLRP1	NLRP2	NLRP3
NOD2	NOSIP	NOTCH1	NOTCH2	NOTCH3	NPPB	NPPC	NPR1	NPR2	NPR3
NR1H2	NR1H3	NR1H4	NR3C1	NRG1	NRG4	NRIP3	NRXN1	NRXN3	NTRK2
OAS1	OAS2	OAS3	OASL	OLFM4	OLR1	OSM	OSMR	OXER1	OXGR1
P2RX5	P2RY12	PARP1	PCNA	PDCD1	PDCD1LG2	PDGFA	PDGFB	PDGFC	PDGFD
PDGFRA	PDGFRB	PECAM1	PF4	PGF	PGR	PHLDA2	PIGR	PLA2R1	PLAC8
PNOC	POU5F1	PPARA	PPARD	PPARG	PPBP	PRF1	PROK2	PROKR1	PRSS2
PSAP	PSCA	PTGDR2	PTGDS	PTGES	PTGES2	PTGES3	PTGIS	PTGS1	PTGS2
PTHLH	PTK2	PTK6	PTPRC	PTPRCAP	PTTG1	QRFPR	RAC1	RAC2	RAD51
RAMP1	RAMP2	RAMP3	RARA	RARB	RARG	RARRES1	RARRES2	RB1	RBPJ
REG1A	RELA	RELT	RGCC	RGS1	RGS2	RGS5	RNF43	ROR1	RORA
RPL21	RPL22	RPL32	RPL34	RPL37	RPS4Y1	RSPO1	RSPO2	RSPO3	RUNX3
RXRA	RXRB	RYK	S100A10	S100A2	S100A4	S100A6	S100A8	S100A9	S100B
S100P	SAA1	SAA2	SAT1	SCG5	SCGB3A1	SEC23A	SEC61G	SELENOP	SELL
SELPLG	SERPINA1	SERPINA3	SERPINB5	SERPINH1	SFN	SIGIRR	SLC2A1	SLC2A4	SLC40A1
SLPI	SMAD2	SMAD3	SMAD4	SMARCB1	SMO	SNAI1	SNAI2	SOD1	SOD2
SOSTDC1	SOX2	SOX4	SOX9	SPARCL1	SPINK1	SPOCK2	SPP1	SPRY2	SPRY4
SQSTM1	SRC	SREBF1	SRGN	SST	ST6GAL1	ST6GALNAC3	STAT1	STAT3	STAT4
STAT5A	STAT5B	STAT6	STMN1	SUCNR1	SYK	TACSTD2	TAGLN	TAP1	TAP2
TBX21	TCL1A	TEK	TFEB	TGFB1	TGFB2	TGFB3	TGFBR1	TGFBR2	THBS1
THBS2	TIE1	TIGIT	TIMP1	TLR1	TLR2	TLR3	TLR4	TLR5	TLR7
TLR8	TM4SF1	TNF	TNFAIP6	TNFRSF10A	TNFRSF10B	TNFRSF10D	TNFRSF11A	TNFRSF11B	TNFRSF12A
TNFRSF13B	TNFRSF14	TNFRSF17	TNFRSF18	TNFRSF19	TNFRSF1A	TNFRSF1B	TNFRSF21	TNFRSF4	TNFRSF9
TNFSF10	TNFSF12	TNFSF13B	TNFSF14	TNFSF15	TNFSF18	TNFSF4	TNFSF8	TNFSF9	TOP2A
TOX	TP53	TPM1	TPM2	TPSAB1	TPSB2	TSC22D1	TSHZ2	TSLP	TTR
TUBB	TUBB4B	TWIST1	TWIST2	TXK	TYK2	TYMS	TYROBP	UBE2C	UCP1
UPK3A	VCAM1	VCAN	VEGFA	VEGFB	VEGFC	VEGFD	VHL	VIM	VPREB3
VSIR	VTN	VWF	WIF1	WNT10B	WNT11	WNT2	WNT2B	WNT3	WNT5A
WNT5B	WNT7A	WNT7B	WNT9A	XBP1	XCL1	XCL2	YBX3	YES1	ZFP36

Supplementary Table S3: Summary of CosMx assay on 7 slides of MTB and NTM samples. FOV: focus of view.

Tissue	MTB1	MTB2	MTB3	NTM1	NTM2	NTM3	NTM4	Total	Mean
Number_of_FOVs	21	47	45	21	15	22	45	216	30.9
Total_Tissue_Area_mm2	8.33	4.65	4.16	3.63	2.09	4.28	5.08	32.2	4.6
Number_of_Cells_in_Final_Analysis	70649	40962	34799	31874	23692	51176	47689	300841	42977
Total_Transcripts_Assigned_to_Cells	8768373	7013069	4749647	4267383	1882347	5634413	7876583	40191815	5741688
Mean_Transcripts_per_Cell	124.1	171.2	136.5	133.9	79.5	110.1	165.2	920.5	131.5
Maximum_Transcripts_per_Cell	2226	2079	1697	2339	728	1362	2944	13375.0	1910.7
Mean_Unique_Genes_Per_Cell	70.14	65.82	58.73	81.5	54.69	69.42	79.18	479.5	68.5
Mean_Transcripts_per_um2	0.0357	0.0222	0.0178	0.0458	0.0323	0.0466	0.0228	0.2	0.0

Supplementary Table S4: Cell population in CosMx assay on 7 slides of MTB and NTM samples.

Cell types	MTB1	MTB2	MTB3	NTM1	NTM2	NTM3	NTM4	overall_ percentage
activated.dendritic.cell	0.71	0.15	0.25	0.36	1.75	0.34	1.46	0.72
alveolar.epithelial.cell.type.1	0.94	0.53	1.36	1.4	5.18	1.05	14.12	2.76
alveolar.epithelial.cell.type.2	6.48	8.67	4.26	9.7	5.88	7.49	3.95	6.72
B.cell	3.97	10.71	6.36	19.78	9.82	2.82	6.77	7.87
B.cell.lineage	5.63	17.05	16.73	5.54	11.32	14.11	10.89	11.19
blood.vessel.cell	3.38	2	1.62	6.5	6.13	4.81	5.28	4.16
CD4+.T.cell	3.98	5.24	5.39	6.38	1.4	5.09	0.97	4.07
CD8+.cytotoxic.T.cell	3.24	1.42	1.76	2.75	7.23	1.2	3.16	3.12
ciliated.cell	0.88	0.1	0.24	0.84	0.39	0.22	4.96	0.83
dendritic.cell.type.1	1.06	2.68	1.86	1.49	1.1	0.69	2.05	1.45
dendritic.cell.type.2	1.71	3.13	4.55	5.09	1.64	4.15	1.5	2.95
fibroblast_a	1.07	4.53	4.58	0.61	4.46	4.59	5.24	3.36
fibroblast_b	2.06	11.41	17.16	17.7	16.12	19.73	10.74	12.61
fibroblast_c	21.16	1.29	1.69	0.37	0.43	2.82	0.84	5.97
lymph.vessel.cell	1.48	1.81	1.21	0.95	0.89	0.78	0.81	1.18
macrophage_a	15.32	0.16	0.24	0.14	0.2	1.17	0.84	3.95
macrophage_b	12.67	0.11	0.3	0.53	0.63	0.89	0.35	3.36
macrophage_c	0.86	6.17	3.45	1.53	7.26	5.11	9.36	4.39
macrophage_d	0.25	2.36	6.79	7.16	5.03	1.16	2.78	3.18
mast.cell	0.95	0.42	0.28	1.33	0.97	0.95	0.92	0.84
muscle.cell	0.31	1.14	0.64	2.04	2.67	0.45	2.92	1.27
natural.killer.cell	0.99	3.42	6.39	1.16	1.91	7.19	3.5	3.3
neutrophil	1.17	1.39	2.53	2.44	0.38	6.36	1.11	2.18
plasma.cell	1.51	11.47	8.01	1.36	3.1	4.33	2.21	4.38
plasmacytoid.dendritic.cell	1.61	2.38	1.94	2.08	1.59	2.08	1.3	1.85
regulatory.T.cell	6.61	0.24	0.4	0.75	2.51	0.41	1.96	2.36